AD-A168 084 OPTICAL FILTERING TECHNIQUES(U) CALIFORNIA INST OF TECH 1/1
PASADENA D PSALTIS MAR 86 RADC-TR-86-2
F30602-81-C-0206

UNCLASSIFIED F/G 9/3 NL

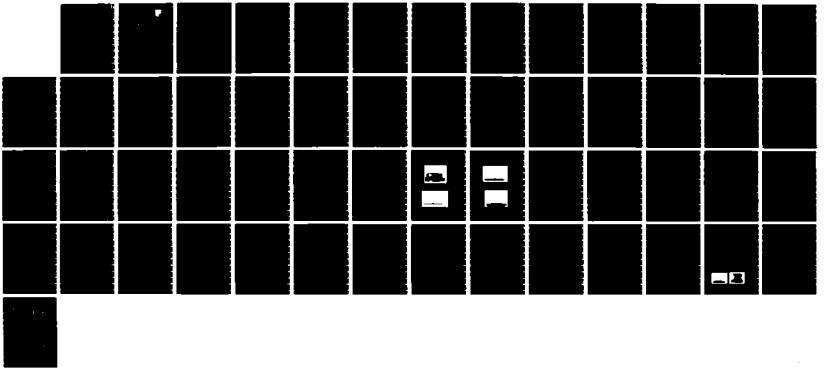

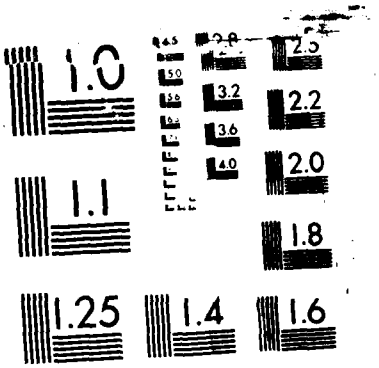

MICROCOPY RESOLUTION TEST CHART

RADC-TR-86-2
Final Technical Report
March 1986

OPTICAL FILTERING TECHNIQUES

California Institute of Technology

Dr. Demetri Psaltis

APPROVED FOR PUBLIC RELEASE; DISTRIBUTION UNLIMITED

ROME AIR DEVELOPMENT CENTER
Air Force Systems Command
Griffiss Air Force Base, NY 13441-5700

This report has been reviewed by the RADC Public Affairs Office (PA) and is releasable to the National Technical Information Service (NTIS). At NTIS it will be releasable to the general public, including foreign nations.

RADC-TR-86-2 has been reviewed and is approved for publication.

APPROVED: Richard D. Hinman

RICHARD D. HINMAN
Project Engineer

APPROVED: William H. Niles

WILLIAM H. NILES, Colonel, USAF
Chief, Communications Division

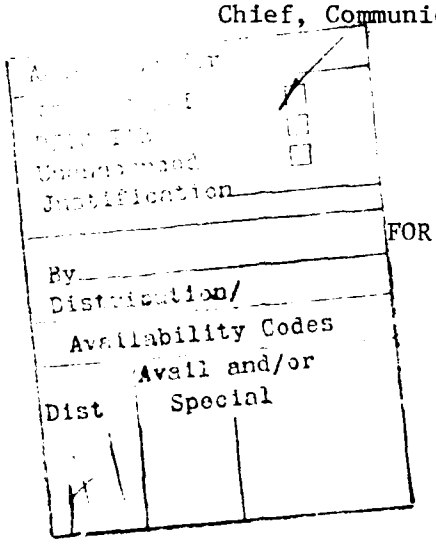

FOR THE COMMANDER: Richard W. Pouliot

RICHARD W. POULIOT
Plans & Programs Division

If your address has changed or if you wish to be removed from the RADC mailing list, or if the addressee is no longer employed by your organization, please notify RADC (DCCD) Griffiss AFB NY 13441-5700. This will assist us in maintaining a current mailing list.

Do not return copies of this report unless contractual obligations or notices on a specific document requires that it be returned.

REPORT DOCUMENTATION PAGE

1a REPORT SECURITY CLASSIFICATION UNCLASSIFIED	1b RESTRICTIVE MARKINGS N/A
2a SECURITY CLASSIFICATION AUTHORITY N/A	3 DISTRIBUTION / AVAILABILITY OF REPORT Approved for public release; distribution unlimited.
2b DECLASSIFICATION / DOWNGRADING SCHEDULE N/A	
4 PERFORMING ORGANIZATION REPORT NUMBER(S) N/A	5 MONITORING ORGANIZATION REPORT NUMBER(S) RADC-TR-86-2
6a NAME OF PERFORMING ORGANIZATION California Institute of Technology 6b OFFICE SYMBOL (If applicable)	7a NAME OF MONITORING ORGANIZATION Rome Air Development Center (DCCD)
6c ADDRESS (City, State, and ZIP Code) Pasadena CA 91125	7b ADDRESS (City, State, and ZIP Code) Griffiss AFB NY 13441-5700
8a NAME OF FUNDING / SPONSORING ORGANIZATION Rome Air Development Center 8b OFFICE SYMBOL (If applicable) (DCCD)	9 PROCUREMENT INSTRUMENT IDENTIFICATION NUMBER F30602-81-C-0206
8c ADDRESS (City, State, and ZIP Code) Griffiss AFB NY 13441-5700	10 SOURCE OF FUNDING NUMBERS PROGRAM ELEMENT NO: 62702F; PROJECT NO: 4519; TASK NO: 42; WORK UNIT ACCESSION NO: P1

11 TITLE (Include Security Classification)
OPTICAL FILTERING TECHNIQUES

12 PERSONAL AUTHOR(S)
Dr. Demetri Psaltis

13a TYPE OF REPORT	13b TIME COVERED	14 DATE OF REPORT (Year, Month, Day)	15 PAGE COUNT
Final	FROM Jan 85 TO Jun 85	March 1986	60

16 SUPPLEMENTARY NOTATION
N/A

17 COSATI CODES			18 SUBJECT TERMS (Continue on reverse if necessary and identify by block number)
FIELD	GROUP	SUB GROUP	Optical Processing Signal Processing Adaptive Processing
17	02	03	
20	06		

19 ABSTRACT (Continue on reverse if necessary and identify by block number)

The purpose of this study was to examine the potential of using optical information processing technology for adaptive antenna beamforming and null steering. The adaptive beamforming/null steering problem consists of estimation of the covariance matrix of the noise field and inversion of the covariance matrix to obtain the antenna element weights which optimize the antenna's directional characteristics (gain pattern). This report examines the adaptive beamforming/nulling problem in view of the capabilities of optics and identifies areas where optics can be used to benefit.

20 DISTRIBUTION / AVAILABILITY OF ABSTRACT	21 ABSTRACT SECURITY CLASSIFICATION
☐ UNCLASSIFIED/UNLIMITED ☒ SAME AS RPT ☐ DTIC USERS	UNCLASSIFIED
22a NAME OF RESPONSIBLE INDIVIDUAL Richard D. Rinman	22b TELEPHONE (Include Area Code) (315) 330-3224
	22c OFFICE SYMBOL RADC (DCCD)

DD FORM 1473, 84 MAR 83 APR edition may be used until exhausted
All other editions are obsolete

OPTICAL FILTERING TECHNIQUES

The purpose of this study is to examine the potential of using optical information processing technology for adaptive beamforming. The work reported here is a continuation of the work described in the report RADC-TR-85-80. One of the conclusions that we reached in the first part of the program is that adaptive broadband phased array processing is an area where analog, accustooptic signal processing technology could be fruitfully applied. Our work during the second phase of this program which is reported here has been concentrated in this area.

A schematic diagram of a broadband phased array is shown in Fig. 1. It consists of N antenna elements with each element having n delayed taps in time. This allows both temporal and spatial processing to be performed, a capabiltity that is essential in the broadband case for two reasons. First, we require multiple taps in the broadband case simply in order to do beamforming, i.e. point the antenna in the direction where the signal is coming from. In addition, the multiple taps allow us to place nulls in the antenna pattern in any direction and any frequency at which there is unwanted interference. The multiple taps provide additional degrees of freedom that increase the total number of jammers (distributed in frequency and angle) that can be cancelled to nN. Equally important, the multiple taps allow us to optimally cancel any jamming waveform within the bandwidth of the signal. In an adaptive implementation of such an array the optimum nN weights should be continuously calculated.

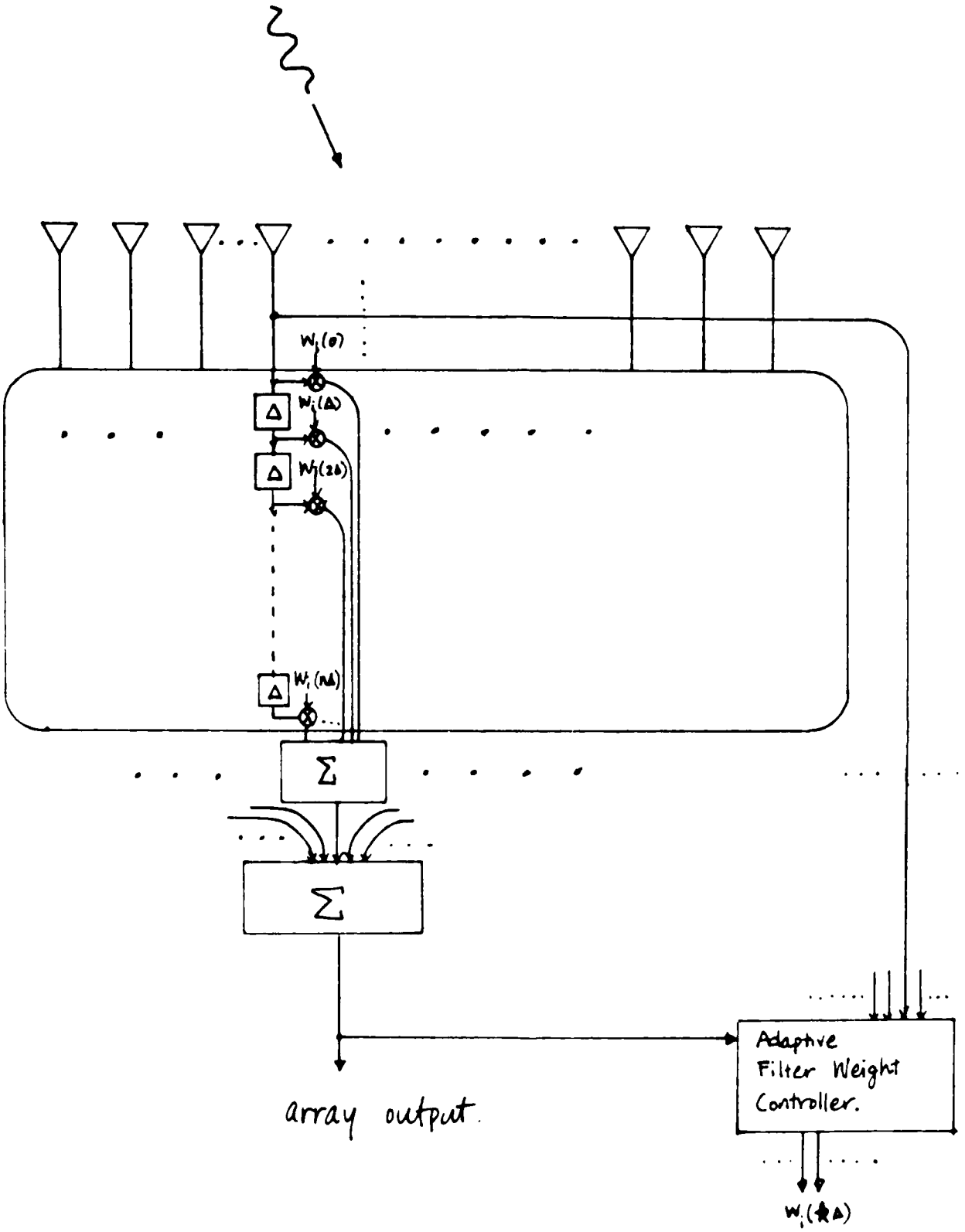

Figure 1. Broadband, adaptive phased array.

This can be accomplished by forming the nN X nN covariance matrix of all the signals at each tap and each antenna element, and multiplying the inverse of the covariance matrix with the steering vector to obtain the optimum weights. In the previous report we have argued that at present there is no efficient method for optically inverting matrices with suitable accuracy. A digital implementation of such a matrix inversion would also be very difficult because of the very large covariance matrices involved in a broadband phased antenna array. We have thus concentrated on the optical implementation of iterative algorithms. In this case the optimum weights are estimated by multiplying the output of the antenna with each delayed signal in all the antenna elements, low pass filtering the result, and subtracting it from the steering signal. Let s(t) denote the output signal of the antenna and let $s_i(t-j\Delta)$ be the signal at the ith antenna element and the jth tap. Then

$$s(t) = \sum_i \sum_j w_i(j) s_i(t-j\,\Delta), \qquad (1)$$

where $w_i(j)$ is the weight at the jth tap of the ith antenna element. The weights are calculated as follows:

$$w_i(j) = S^*_i(j) - G \int_{t-T}^{t} s(t') s_i(t'-j\Delta) dt', \qquad (2)$$

where $S_i(j)$ is the steering vector and G is the feedback gain. When equations (1) and (2) are simultaneously satisfied, i.e. when steady state has been reached, the weights that are calculated by Eq.(2) are approximately equal to the optimum weights. Moreover, if none of the eigenvalues of the noise

covariance matrix are zero and the feedback gain is sufficiently low then the iterative loop will converge to this optimum solution.

The operation that needs to be performed to implement equation (1) is a multichannel one dimensional convolution (the summation over the index j) followed by a summation across the different channels to produce the signal s(t). Equation (2) is also a multichannel system that correlates s(t) with the signals received in each antenna element and continuosly produces estimates of all the weights. The weights are then subtracted from the steering signal and fed back to equation (1) for continuous iteration. This is shown in block diagram form in Figure 2, with the symbol * denoting correlation and ✱ denoting convolution. The operations required for the implementation of the block diagram in figure 2 are very well matched with the capabilities of optical signal processing systems. One dimensional correlations and convolutions can be readily implemented with acoustooptic devices, the only mature spatial light modulators that are presently available. The multichannel capability can be implemented by making use of the third dimension that is available in an optical system through multiple transducer acoustooptic devices. Multichannel acoustooptic devices have been developed relatively recently and they are not as well understood and characterized as single channel devices . However, devices with up to 32 channels and bandwidth in excess of 100 MHz are commercially available and a larger number of channels is within the capabilities of current technology. Thus,

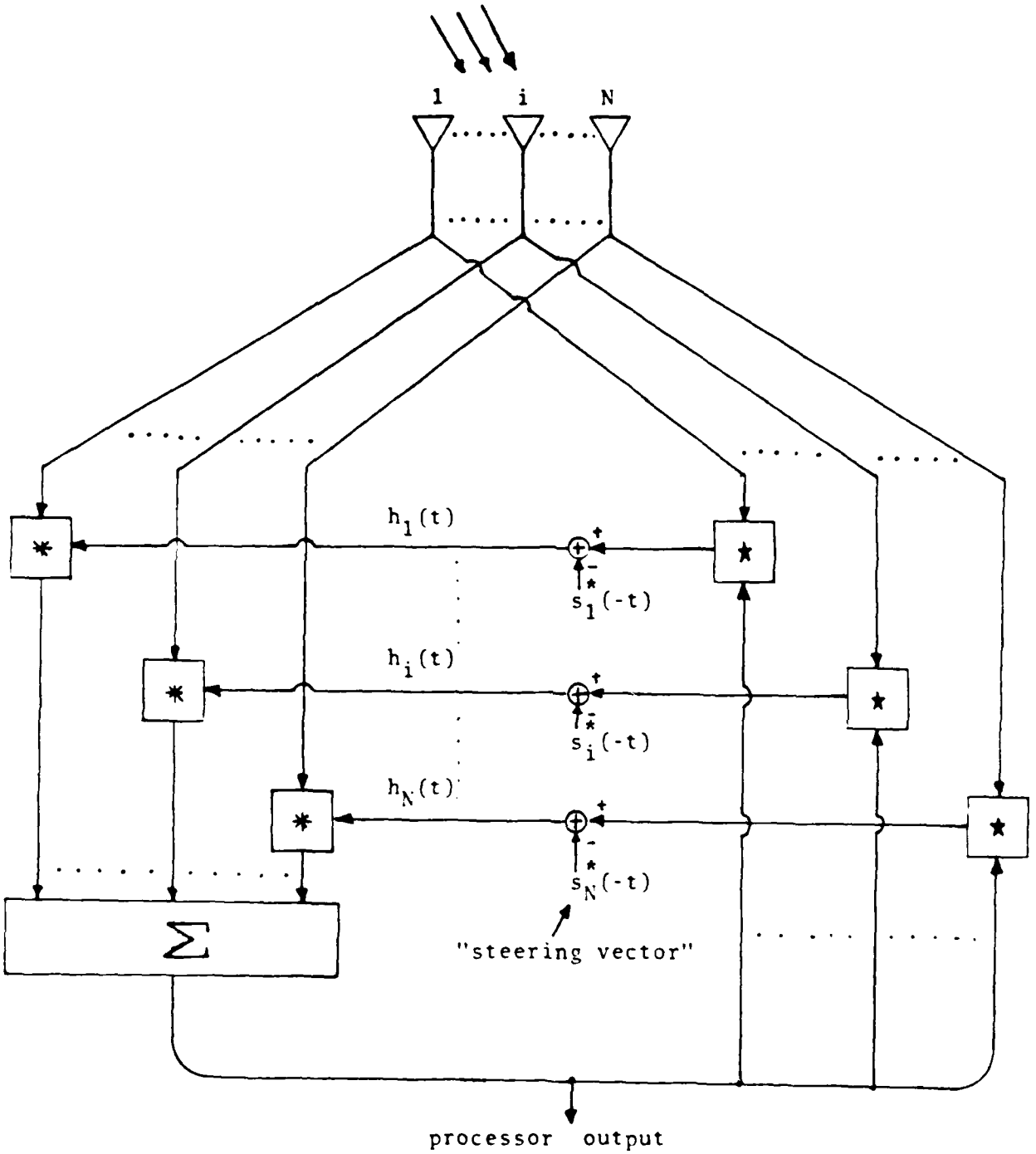

Figure 2. Signal processing requirements for a broadband adaptive phased antenna array.

we estimate that multichannel acoustooptic technology is now or will be in the near future sufficiently well developed for this application. A careful examination of the properties of multichannel AO devices ought to be undertaken however in order to estimate the expected performance of a broadband acoustooptic adaptive array processor that is implemented with them.

Having identified in principle the general approach for building an adaptive, broadband phased array processor using multichannel acoustooptic technology, we now turn to the choice of specific architectures. There are two basic methods to perform convolutions/correlations with acoustooptics: space or time integration. There are also several possible variations of each basic architecture. In making an appropriate choice for this application we must first take into consideration the fact that all the input signals to the correlators and the convolvers need to be dynamic. This fact narrows the choise considerably. Secondly, the correlator and convolver blocks need to be compatible; the output of the convolvers becomes the input to the correlators and vice versa. Space integrating systems produce the output as a function of time whereas time integrating systems produce it as a function of space. Thus space integrating systems are relatively more staightforward to use because we can readily address an acoustooptic device with the temporal signal that is produced by them. The output of a time integrating processor is typically detected as a function of space on a detector array. The relatively slow read-out of the detector that converts the detected signal to a temporal electronic signal makes the use of

time integrating processors that utilize detector arrays impractical. There is an alternative solution however which involves the use of optically addressed spatial light modulators which can act as time integrating detectors and simultaneously as light modulators. This allows the same device to be used both as an output device for one system and an input device for the second. We have investigated the possibility of using nonlinear optical crystals to accomplish this goal. The results of this investigation, presented in the paper attached as Appendix A to the report, are very encouraging and we have used this technique in the implementation of adaptive filters as we will discuss later.

Even with the restrictions mentioned above we are still left with considerable flexibility. We can select a purely space integrating approach where both the convolution and the correlation are performed with space integrating processors or a purely time integrating approach. Finally, hybrid approaches are possible where time integration is used for one of the processors and spatial integration for the other. Actually three of these four possible combinations have potential merit and we have explored them in some detail. The only possibility that does not seem to be useful is a fully time integrating approach.

The purely space integrating approach involves the use of counter propagating multichannel acoustooptic devices to perform the convolution whereas the correlations are performed with copropagating acoustooptic devices. This system is described in

detail in the paper attached as Appendix B to this proposal. The second approach we have considered is the use of time integrating correlations combined with space integrating convolvers. This approach has been previously investigated by Rhodes and Penn who utilized optically addressed spatial light modulators (e.g. the Hughes liquid crystal light valve) as the time integrating detector for the correlator part of the system and also as a spatial light modulator for the space integrating convolver section. We have investigated the possibility of using photorefractive crystals for the same purpose. The results of this investigation are described in the paper attached as Appendix C. The advantages of photorefractive crystals are very high resolution, excellent optical quality and contollable integration time. A disadvantage of the photorefractive crystals that is shared by the optical spatial light modulators is the relatively long response time (a hundred milliseconds or more) which translates to long adaptation time. The emergence of new photorefractive materials, such as GaAs, with much faster response time than the BSO crystal used in our experiments promises to alleviate this problem.

The third and final possibility we explored is the use of a time integrating convolver and a space integrating correlator. We will consider a single channel version of this system that performs only temporal adaptive filtering. This system can be extended to spatial and temporal filtering through the use of the third dimension and multichannel acoustooptic technology in a

manner completely analogous to the systems described earlier. We will describe the operation of the system for the active case where we are looking for a known signal s(t) and jammers are present. The optical system is shown in Figure 3. The input signal x(t) is used to temporally modulate the laser diode in the time integrating portion of the system and it is also applied as the input to the acoustooptic device in the space integrating portion of the system. The input to the acoustooptic device in the time integrating part of the system is the signal s(t) minus the output signal from the space integrating system amplified by the gain G. The time integrating correlation forms as an optical spatial modulation function on the nonlinear crystal. This signal is then convolved with the input signal x(t) in the space integrating part of the system. The output of the system is the signal e(x/v) that forms on the nonlinear crystal and it can be written as

$$e(x/v) = \int x(t)[s(t-x/v)-Gx'(t-x/v)]dt$$
$$x'(t) = \int x(t-x/v)e(x/v)dx. \qquad (3)$$

Taking the Fourier transform of the above equations and solving for the transform of the of the output signal E(w), we obtain:

$$E(w) = X(w)S^{*}(w)/(1+G|N(w)|^{2}) \qquad (4)$$

where $|N(w)|^2$ is the power spectrum of the noise at the input and we have neglected the effects of the finite windows of the acoustooptic devices and the finite integration time of the nonlinear crystal. This system is in many ways similar to the

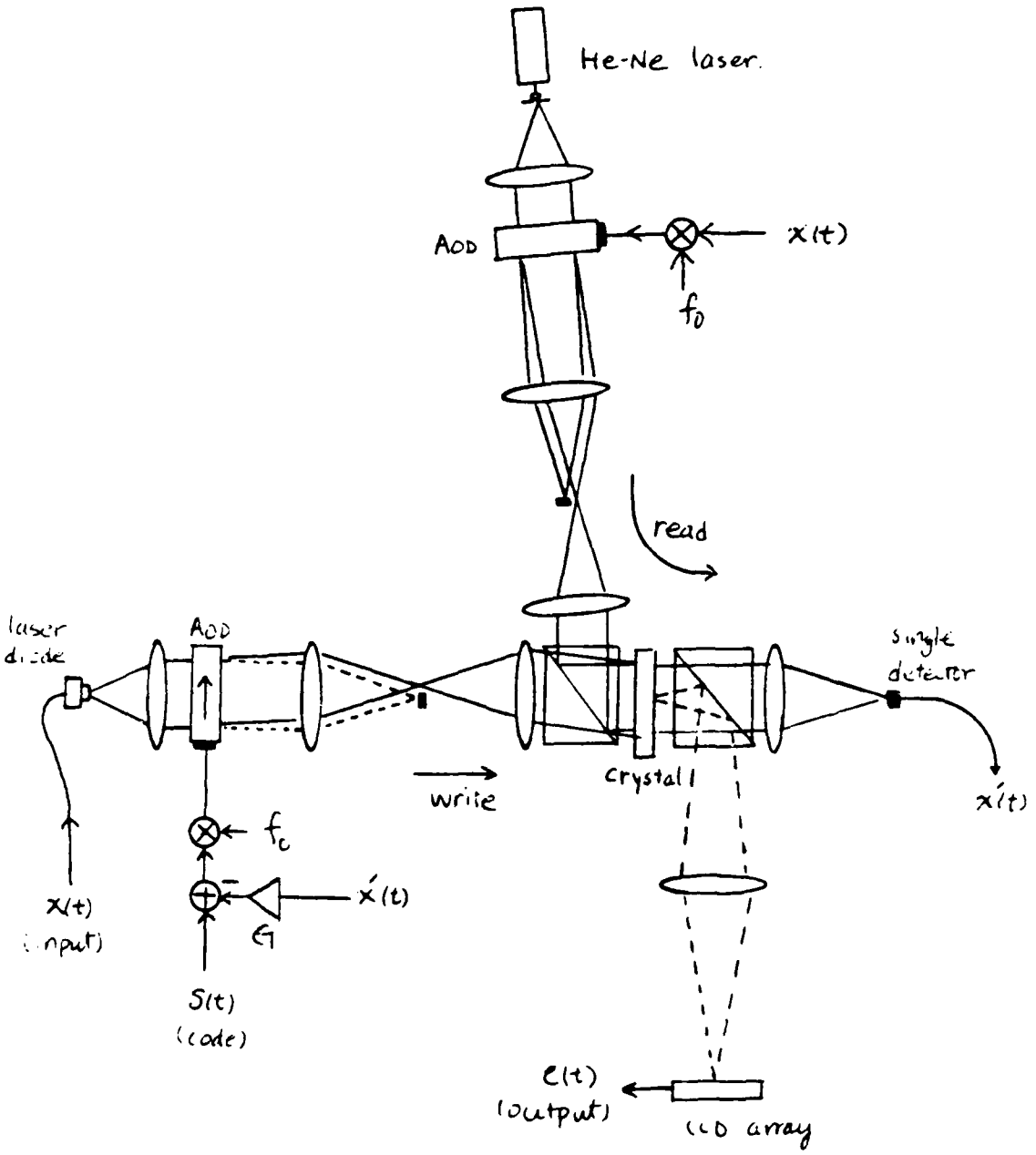

Figure 3. Time integrating correlator with space integrating cancellation loops.

system described in appendix C with the important distinction that now the primary filter is time integrating whereas the space integrating system is in the feedback loop. This allows very long codes s(t) to be correlated as it would be required in a spread spectrum application.

The characteristics of the adaptive filters we have been discussing are in general excellent in terms of achievable bandwidth, number of antenna elements and number of taps per element (i.e. total number of degrees of freedom), overall power consumption and size. The adaptation speed is slow for the time integrating approach with currently available nonlinear crystals or optically addressed spatial light modulators, but it is very fast in a space integrating implementation. The principal remaining question is the maximum null depth that can be achieved with these analog implementations. There are two main factors that limit this performance criterion: the limited dynamic range of the devices used and instabilities in the feedback loop caused by phase distortions in the optical system. This issue is addressed in appendix C, but we will briefly summarize our findings here. In the space integrating approach the maximum null depth that can be achieved in the absence of phase distortion is essentially equal to the dynamic range of the detectors used in the system. These detectors can have in excess of 80dB dynamic range; hence if we are willing to use a sufficiently powerful light source to utilize fully the detector dynamic range, then we can in principle achieve very deep nulls. In our experiments

however the phase errors in the feedback loop cause oscillations to occur before the dynamic range limits are reached. These phase errors occur for entirely different reasons in the different approaches but they have precisely the same effect: If the feedback gain is sufficiently increased we reach a condition of positive feedback that can sustain oscillation at some frequencies within the bandwidth. Thus the first priority in building a system of this type with very high jammer suppression is to find ways to have a flat phase response over the entire bandwidth through choice of the architecture and clever design rather than increasing the dynamic range of the devices used.

APPENDIX A

A BIAS FREE TIME INTEGRATING OPTICAL CORRELATOR USING A PHOTOREFRACTIVE CRYSTAL

Demetri Psaltis, Jeffrey Yu, and John Hong
Department of Electrical Engineering
California Institute of Technology
Pasadena, California 91125

Abstract

An acousto-optic time integrating correlator is demonstrated using a photorefractive crystal as the time integrating detector.

I. Introduction

Time integration[1] has proven to be a powerful technique in optical signal processing and has been used in a wide variety of architectures. A major drawback of time integrating processors is the buildup of bias in additon to the signal. This occurs because the photogenerated charge that is integrated on the detector is proportional to the intensity of the optical signal which makes it necessary to represent bipolar signals on a bias. The effective system dynamic range at the output is given by DR' = DR (SBR/(1+SBR)) where DR is the dynamic range of the output detector and SBR is the signal to bias ratio on the detector.[2] In most cases of interest, the SBR is much smaller than unity and thus the added bias significantly reduces the usable dynamic range of the system.

The most frequently used method for separating the signal from the bias involves placing the signal on a spatial carrier and then electronically filtering the output of the integrator. This method of bias removal, however, does not solve the dynamic range problem since the processing is done after the detection of the signal. Also, an additional constraint is placed on the resolution of the detector, since the pixel separation must be less than one half of the period of the carrier being recorded, which will result in a significant reduction in the available space-bandwidth product at the output.

In this paper, a new method for performing time integrating correlation is described using a photorefractive Bismuth Silicon Oxide (BSO) crystal as the time integrating element. The correlation is formed on a spatial carrier in the crystal and read out with an auxillary beam. Since only the signal recorded on a spatial carrier is stored in the photorefractive crystal, the diffracted light that is detected contains the correlation information without the bias. The bias does not reduce the dynamic range of the output detector used for final readout, but rather the diffraction efficiency of the BSO crystal. In addition, the resolution of the BSO crystal is very much higher than that of a CCD detector, allowing the correlation of very high space-bandwidth signals to be formed on a carrier. Finally, since the result of the time integrating correlator is read-

out optically, the output can be easily interfaced with other optical systems, thus making new architectural designs possible.

In section II, the theory of optical recording in photorefractive crystal is reviewed and extended to the use of photorefractive crystals as time integrating elements. The architecture and experimental results are described in section III. Dynamic range, linearity, system limitations, and other performance aspects are discussed in section IV.

II. Photorefractive Crystals as Time Integrating Optical Detectors

When a photorefractive BSO crystal is illuminated by an intensity grating, electrons are excited *from traps into* the conduction band. These charges migrate due to diffusion and drift from an externally applied electric field and then recombine in dark regions, creating a spatially varying internal space-charge field. This field modifies the index of refraction in the crystal through the linear electrooptic effect and as a result, a holographic phase grating is recorded in the crystal. Grating formation in photorefractive media has been extensively studied and modeled[3,4]. We will show here that the photorefractive crystal acts as a time integrating element.

Let the intensity incident on the crystal be as follows:

$$I(x,t) = \begin{cases} I_0 + \mathrm{Re}\{I_1(x,t)e^{ikx}\} & \text{for } t>0 \\ 0 & \text{otherwise} \end{cases} \qquad (1)$$

Assuming that self diffraction effects are negligible and that the spatial variations of $I_1(x,t)$ are small compared to the grating frequency k, then the intensity of the light that is diffracted when the crystal is illuminated by a read-out beam can be shown to be:[5]

$$I_{out}(x,t) = \left| \frac{K_1}{\tau} e^{-t/\tau} \int_0^t \frac{I_1(x,t')}{I_0} e^{t'/\tau}\, dt' \right|^2 I_R \quad . \qquad (2)$$

I_R is the intensity of the readout beam and K_1 is a complex constant involving the material parameters of the crystal, the grating frequency, and the applied electric field. τ is the complex time constant of the space charge field and is given by[3] $\tau = K_2/I_0$. K_2 is also a complex constant that depends on the photorefractive material used and the experimental conditions. I_0 is the average light intensity incident on the crystal during exposure.

If $I_1(x,t)$ is expanded into its temporal Fourier components,

$$I_1(x,t') = \int_{-\infty}^{\infty} \tilde{I}_1(x,w)\, e^{iwt'}\, dw,$$

then the output intensity for $t \gg \tau$ can be written as follows:

$$I_{out}(x,t) \approx \left| \frac{K_1}{\tau I_0} \int_{-\infty}^{\infty} \frac{\tilde{I}_1(x,w)}{(1/\tau + iw)}\, e^{iwt}\, dw \right|^2 I_R \qquad (3)$$

The above is recognized to be a low pass filter with cut-off frequency $1/|\tau|$, which is approximately equivalent to the output of a sliding window integrator, with integration time τ. Thus,

$$I_{out}(x,t) \cong \left| \frac{K_1}{\tau} \int_t^{t+\tau} \frac{I_1(x,t')}{I_0} dt' \right|^2 I_R \qquad (4)$$

Hence, the output intensity can be treated as the square of the normalized integration of the signal I_1. An interesting observation is that if $I_1(x,t)$ were independent of time, then the output intensity depends only on the ratio of the modulated intensity I_1 to the DC intensity I_0.

III. Experimental Demonstration

A schematic diagram of the experimental system is shown in Fig 1. The input electrical signals are mixed with the center frequency of the acousto-optic devices (AODs) and fed into the AODs. The first AOD is illuminated by a collimated wave and the upshifted diffracted order is imaged onto the second AOD, then reimaged onto the photorefractive BSO crystal. The second AOD is oriented such that the acoustic signal is counterpropagating with respect to the image of the acoustic signal from the first AOD. The undiffracted light transmitted through the first AOD is incident at the Bragg angle of the second AOD. The upshifted diffracted order of the second AOD is also imaged on to the BSO crystal. The undiffracted light is spatially filtered before reaching the

BSO crystal. In this arrangement, the AODs are parallel to each other , but the diffracted orders propagate at an angle with respect to each other even though both diffracted beams are temporally upshifted. This causes the signals from the two AODs to interferometrically record the correlation signal on the BSO crystal at a high spatial frequency. Let the inputs to the AODs be

$$v_1(t) = a(t)e^{iw_0t}$$

$$v_2(t) = b(t)e^{iw_0t},$$

where $w_0/2\pi$ is the center frequency of the AOD. The intensity incident on the photorefractive crystal is

$$\begin{aligned} I(x,t) &= |a(t-x/v)e^{i\gamma x} + b(t+x/v)e^{-i\gamma x}|^2 \\ &= |a(t-x/v)|^2 + |b(t+x/v)|^2 + \\ &\qquad 2\,\mathrm{Re}\{a(t-x/v)b^*(t+x/v)e^{i2\gamma x}\}, \end{aligned} \tag{5}$$

where v is the acoustic velocity of the AOD and $\gamma = w_0/v$. We will treat the case where $|a(t)|^2$ and $|b(t)|^2$ can both be approximated as constants, as is the case for FM signals. Then, the intensity pattern can be separated into a DC term I_0 and a signal term $I_1(x,t)$ modulating a spatial carrier $\cos(2\gamma x)$ in the form of Eq. 1. This intensity pattern results in the formation of a hologram on the photorefractive crystal as described in the previous section. The hologram is readout with an auxilary beam and is imaged onto a charge coupled device (CCD) detector for read-out.

If the assumption that $I_1(x,t)$ has spatial frequencies

which are small compared to the carrier frequency 2γ is valid then we can use Eq. 4 to obtain an expression for the output intensity detected by the CCD

$$I_{out}(x) \cong I_R \left| \frac{K_1}{\tau} \right|^2 \left| \int_t^{t+\tau} \frac{a(t-x/v)\, b^*(t+x/v)}{|a|^2 + |b|^2}\, dt \right|^2,$$

and by defining variable $t_1 = t - x/v$

$$I_{out}(x) \propto \left| \int_{t+x/v}^{t+\tau-x/v} a(t_1) b^*(t_1+2x/v)\, dt_1 \right|^2 \qquad (6)$$

Hence the system produces the magnitude square of the correlation between the signals a(t) and b(t) integrated over a finite interval τ.

Flint glass acousto-optic cells driven at a center frequency of 70MHz were used in the experiment. A symmetric linear chirp signal with bandwidth Δf = 5Mhz was fed into each cell to produce the autocorrelation peak. The Bragg angle of the AODs was 0.2°, which corresponded to a grating frequency equal to 35 lines per millimeter in the BSO crystal.

The BSO crystal used in the experiment was cut in the ⟨110⟩ direction and measured 15 x 15 x 2 mm. An external electric field of 7 kV/cm was applied in the ⟨001⟩ direction of the crystal which was also the direction of the grating vector.

The correlation was recorded on the crystal with an Argon laser at a wavelength of 514 nm with average intensity

equal to 1μW/cm^2. The correlation was read-out with a He-Ne laser (λ = 633 nm) with intensity 150 μW/cm^2. Cylindrical lenses (not shown in Fig.1) were used to expand the output of the AODs thereby illuminating the full aperture of the BSO crystal and also to focus the diffracted light onto a one dimensional CCD.

The output signal to bias ratio of a conventional time integrating correlator is reduced when the levels of the two signals are unequal and/or if there is additive noise present in the system. Both conditions were simulated experimentally. Noise was simulated by adding a 70MHz signal to the input of one of the AODs. The output of a standard time integrating correlator (i.e. the correlation formed directly on the CCD), for the noise free case and equal amplitude signals is shown in Fig 2. This condition provides the maximum signal to bias ratio for the system. We can see in Fig 2 that, there is still a strong bias term added to the correlation peak. The correlation produced by temporally integrating on the photorefractive crystal is shown in Fig.3. In this case, all the bias due to temporal integration is removed, and any residual bias is due entirely to dark current from the CCD. The outputs of the bias removal correlator with input signal to noise ratios of 0dB and -10dB are shown in Figs 4 and 5, respectively. Again, bias levels which appear in the figures were entirely due to the integration of dark current in the output detector. In

practice, the detector dark current can be minimized by increasing the intensity of the readout beam, thereby decreasing the required integration time of the output CCD detector and/or cooling the detector.

III. Performance

The experimental results described in the previous section show a dramatic qualitative improvement in the correlation that is obtained when the photorefractive crystal is used instead of the CCD. In this section, we examine certain characteristics of this method which are useful for quantitatively evaluating its performance. Specifically, we examine the linearity, integration time, dynamic range, and sensitivity of the correlator.

1) Linearity

In a conventional time integrating correlator (coherent or incoherent), the output correlation is basically proportional to the signals applied to the AODs. Nonlinearities occur only when we exceed the linear dynamic range of the devices used, i.e. if the diffraction efficiency of the AOD exceeds several percent or the integrating detector is driven to saturation. In the photorefractive time integrating processor, the output intensity is a nonlinear, monotonically increasing function of the input voltage. The nonlinearity arises because of the square law detection at

the final read-out stage and the recording mechanism in the photorefractive crystal. The nonlinear relationship is now studied analytically and experimental verification of the theoretical results is presented.

Let $v_1(t) = s(t)$ be a fixed reference signal and $v_2(t) = as(t)$ be an input signal of varying amplitude ($0<a<1$). Since the correlation term contains spatial frequencies which are much lower than the grating frequency, near the correlation peak ($x=0$) the intensity incident on the photorefractive crystal is

$$I(x,t) = (1 + a^2 + 2a \cos kx)\,|s(t)|^2.$$

Using Eq. 1, the output intensity at the CCD is proportional to

$$I_{out} \propto \left| \frac{2a}{1 + a^2}\,\tau \right|^2 .$$

The modulation depth of the intensity incident on the BSO crystal is

$$m = \frac{2a}{1 + a^2},$$

and hence

$$I_{out} \propto m^2. = 4a^2/(1+a^2). \qquad (7)$$

Fig 6 is a graph of the output intensity at the correlation peak vs. the modulation depth incident on incident on the crystal. The experimental result is in excellent agreement with the square law relationship predicted by Eq. 7.

A plot of the output intensity as a function of the

amplitude of the input signal 'a' is shown in Fig 7. The nonlinear relationship between the input and output signals is generally a disadvantage since the scaling of signals of varying amplitudes will be nonlinear. This, however, will not cause a problem if the correlator is used only as a signal detection device, since correlation peaks will still be discernible and only the threshold level need be adjusted accordingly to maximize the probability of detection.

ii) Integration Time

In a conventional time integrating correlator, the integration time is limited by the dark current build-up on the output detector, typically up to several hundred milliseconds. When the photorefractive crystal is used, the integration time is determined by the rise time of the internal space charge field which can easily be made much longer. The correlation can be read-out at any rate that is convenient by an auxillary detector array.

The integration time is approximately equal to $|\tau|$, where

$$|\tau| = \left| \frac{K_2}{I_0} \right| . \qquad (8)$$

Hence, the integration time of the bias removal correlator can be controlled by varying the writing intensity. This control is important since the integration time can be matched to the length of the reference signal

thereby increasing the probability of detection of a weak signal.

The time reponse of the correlation peak for different values of average incident intensity is shown in Fig. 8. Fig. 9 is a plot of intensity vs the inverse of the experimentally observed rise time. There is excellent agreement between the experiment and equation 8.

The integration time, however, has a finite range over which it can be adjusted. The maximum integration time is limited by the thermal effects in the crystal. If the rate at which carriers are generated thermally become comprable to the rate at which they are photo-generated, then the modulation depth of trap density will be reduced. As a result, the diffraction efficiency of the grating will decrease. In practice, the minimum integration time is limited by the maximum light intensity that is available for recording. The integration time can be reduced to 30ms, if the incident intensity is made equal to $18mW/cm^2$. This power level, however, is simply not practical for most applications.

iii) Dynamic Range and Sensitivity

Since the output of the bias removal correlator is presented without bias, the output dynamic range of the system is essentially equal to the dynamic range of the readout detector array. In order to characterize the performance of the system we need to determine how the input

signal levels are mapped to this output dynamic range. Let the dynamic range of the photorefractive crystal be defined as $DR_{BSO} = m_{max}/m_{min}$, where m_{max} is the maximum modulation depth (m_{max}=1), and m_{min} is the minimum modulation depth for which a diffracted signal is detectable above the output scatter and noise level of the system.

Given two input signals $v_1(t) = a\ s(t)$ and $v_2(t) = s(t)$, the modulation depth of the light incident on the crystal is $m = 2a/(a^2+1)$. Thus, the minimum detectable input signal is given by

$$a_{min} = m_{min}/2 = 1/DR_{BSO}$$

The useful range over which 'a' can vary is limited by DR_{BSO}. From a_{min}, one can define an input dynamic range given by

$$DR_{input} = 1/a_{min}^2 = 4/m_{min}^2$$

The most important parameter in determining the system dynamic range is the minimum detectable modulation depth m_{min}. Experimentally, we measured the dynamic range to be equal to 23dB. This corresponds to a minimum modulation depth of 0.142. We expect that through careful design this can be substantially improved. However, all the mechanisms that determine m_{min} are not fully understood. It is believed that besides detector noise and scattering from the crystal, the modulation depth is limited by thermal effects in the material and shot noise arising from the internal currents.

Another important aspect of the correlator system is its sensitivity or the minimum signal to noise ratio that is

detectable. This parameter is also determined by the minimum detectable modulation depth, m_{min}. Given a reference signal $v_1(t) = a\,s(t)$ and an input signal contaminated by additive noise, $v_2(t) = b\,s(t) + n(t)$, the modulation depth of the intensity incident on the crystal is

$$m = \frac{2ab\,|s(t)|^2}{(a^2+b^2)|s(t)|^2+\sigma_n^2}.$$

The reference level which maximizes m is given by

$$a = (b^2+\sigma_n^2/|s(t)|^2)^{1/2},$$

corresponding to a modulation depth of

$$m = \frac{b}{(b^2+\sigma_n^2/|s(t)|^2)^{1/2}}.$$

In practice, optimizing the reference level can easily be achieved by setting the power of the reference equal to the total average power of the input signal.

Normalizing the signal and noise terms such that $|s(t)|^2 = \sigma_n^2 = 1$ we obtain:

$$m = \frac{b}{(b^2+1)^{1/2}}.$$

Thus, the minimum input SNR that produces a detectable correlation peak at the output is

$$(S/N)_{min} = (b^2/\sigma_n^2)_{min} \approx m_{min}^2.$$

From the experimentally measured value of m_{min}, the correlator should have had a sensitivity of -17dB. However, experimental results showed a sensitivity of -14dB.

IV. Conclusion

The photorefractive time integrating processor that has been described has several advantageous features: bias removal, increase in the output space bandwidth product, and the ability to directly interface the result of the time integrating processor with other optical systems. Bias free correlation is desirable because it allows us to increase the dynamic range and hence the sensitivity of time integrating processors. In the implementation described in this paper, however, the square law detection at the output reduces the available overall dynamic range. A definite improvement in dynamic range can be obtained if the correlation that is formed in the photorefractive crystal is interferometrically detected on the output detector. Another limitation of the system described here is the long integration time (several seconds). In some applications this long integration time is desirable and could result in extremely good sensitivity (detection of signals with very low SNR). However it is certainly desirable to be able to decrease the integration time to several milliseconds. This could be accomplished by increasing the optical power of the writing beams, but this is in general an impractical solution. Another limitation of this technique is the relatively low diffraction efficiency that can be obtained with BSO crystals (2-3%), which reduces the overall light efficiency. Materials with higher electrooptic coefficients, such as Barium Titanate, can

provide better efficiencyμ however, the time constant that is obtained with this particular material is much longer than BSO. New photorefractive materials that are currently being developed and show promise for a large improvement in optical sensitivity as well as higher electrooptic coefficients may provide a very substantial improvement in performance, and specifically, reduce the total optical power that is required.

Acknowledgements

This work is supported by the Air Force Office of Scientific Research and the Army Research Office.

References

1. Sprague, R. A., and D. Koliopoulos **Applied Optics**, 15 89 (1976)

2. Psaltis, D. **Optical Engineering**, 23 12 (1984)

3. Kukhtarev, N. V., V. B. Markov, S. G. Odulov, M. S. Soskin **Ferroelectrics**, 22 949 (1979)

4. Feinberg J., D. Heiman, A. R. Tanguay, R. W. Hellwarth **J. Appl. Phys.**, 51 1297 (1980)

5. Ph. D. Thesis M. Cronin-Golomb, California Institute of Technology March 1983

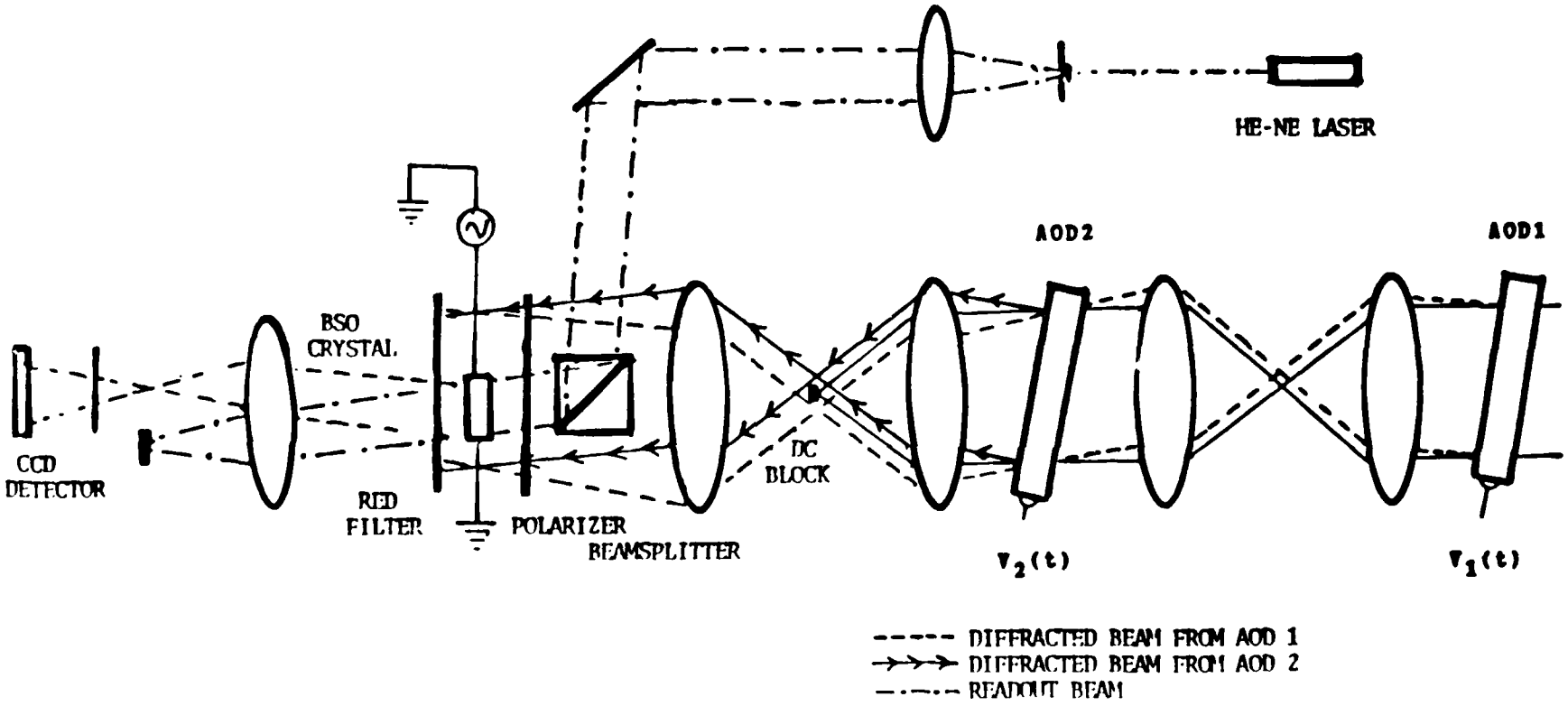

Figure 1 Optical set-up of the photorefractive bias removal correlator

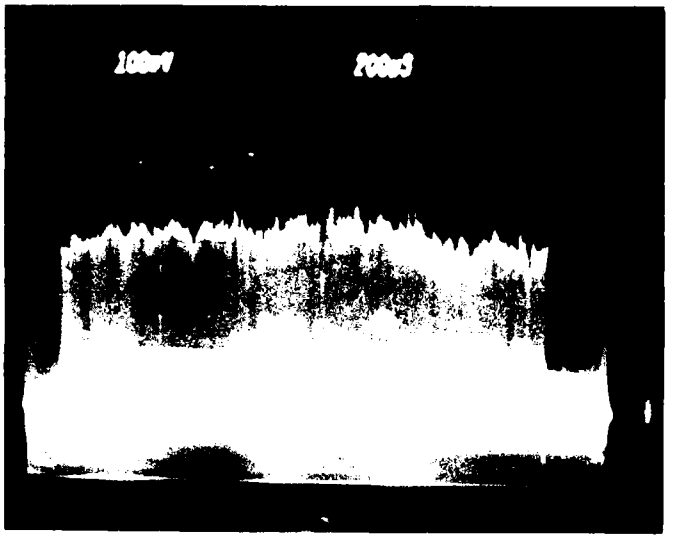

Figure 2. Output of a Standard Time Integrating Correlator without Noise

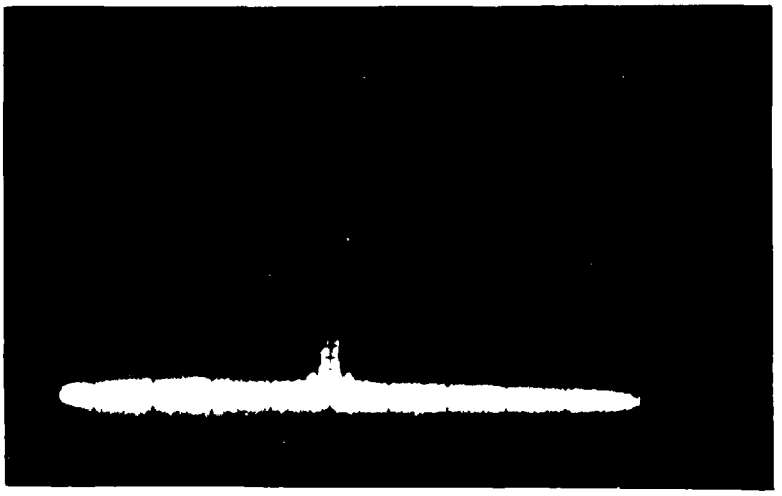

Figure 3. Output of the Bias Removal Correlator without Noise

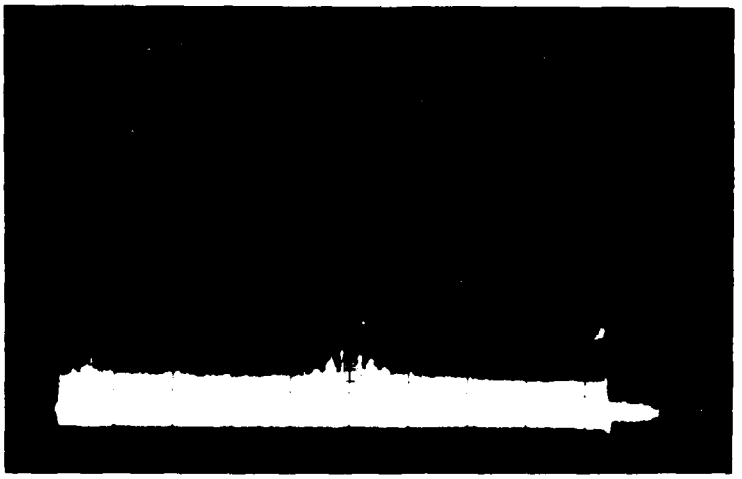

Figure 4. Output of the Bias Removal Correlator with a signal to noise ratio of 0 dB

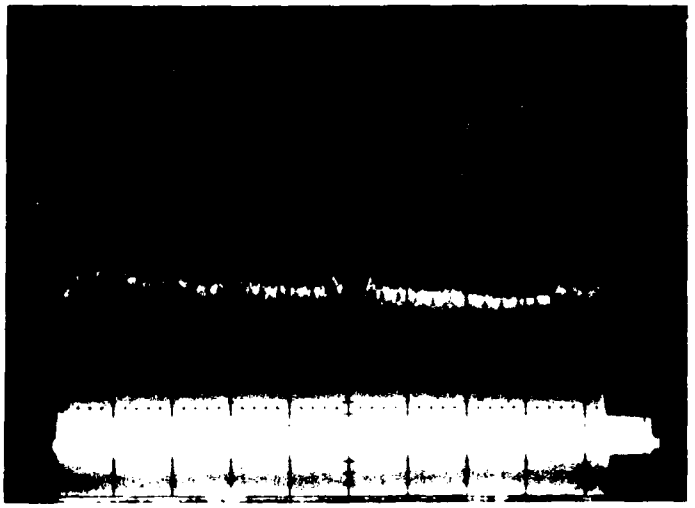

Figure 5. Output of the Bias Removal of Correlator with a signal to noise ratio of -10 dB

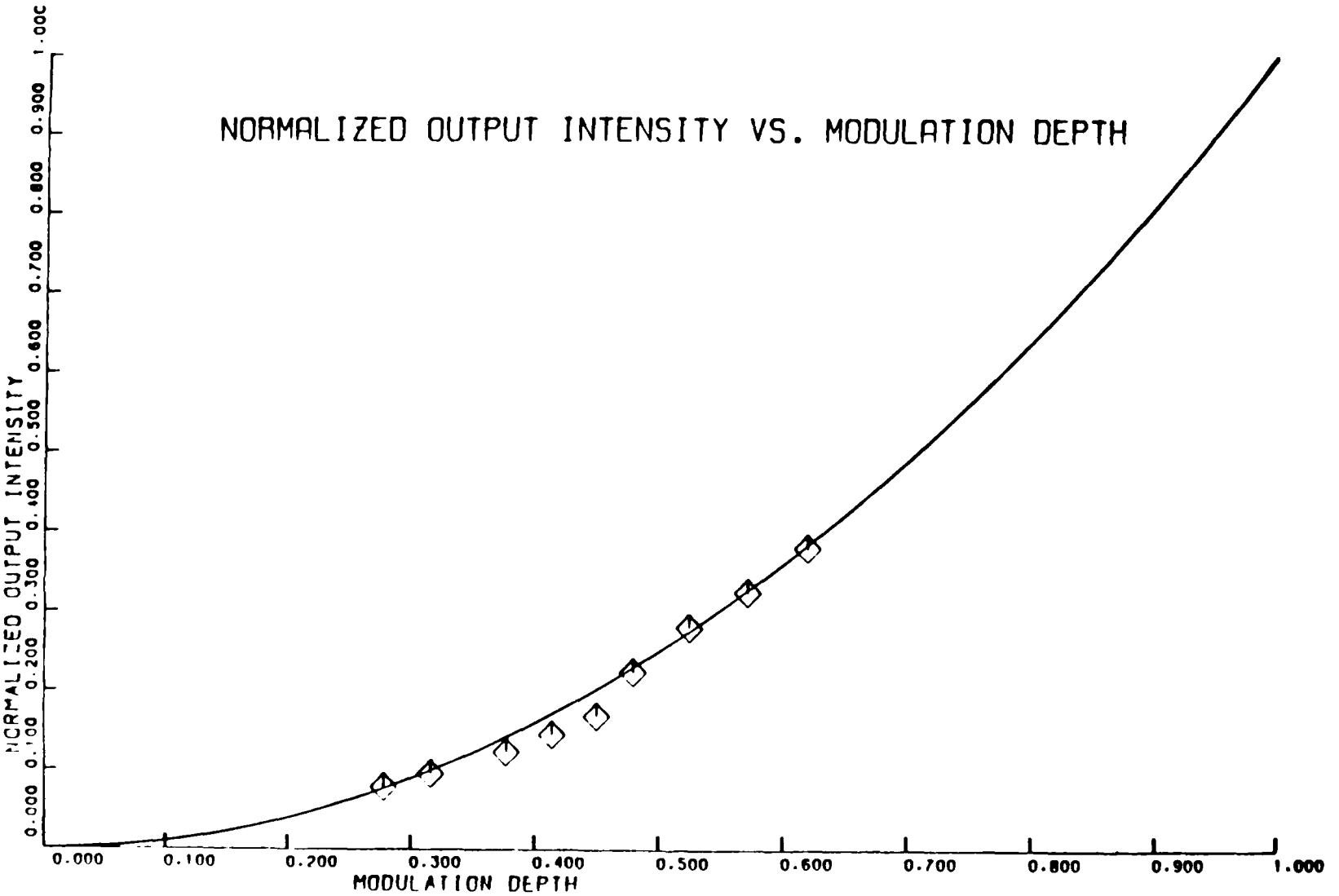

Figure 6 Normalized output intensity vs. modulation depth.

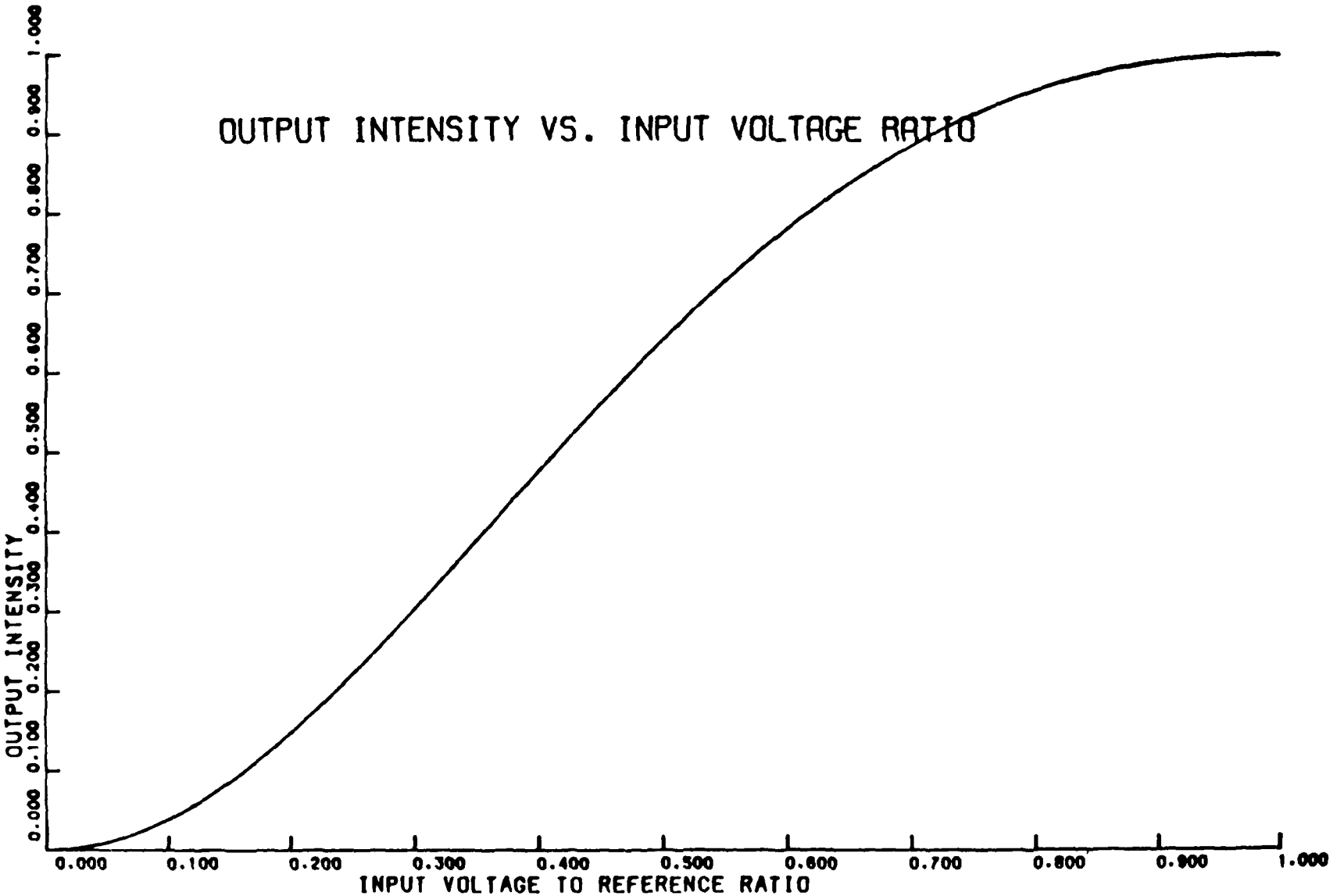

Figure 7 Theoretical plot of output intensity vs. input voltage ratio.

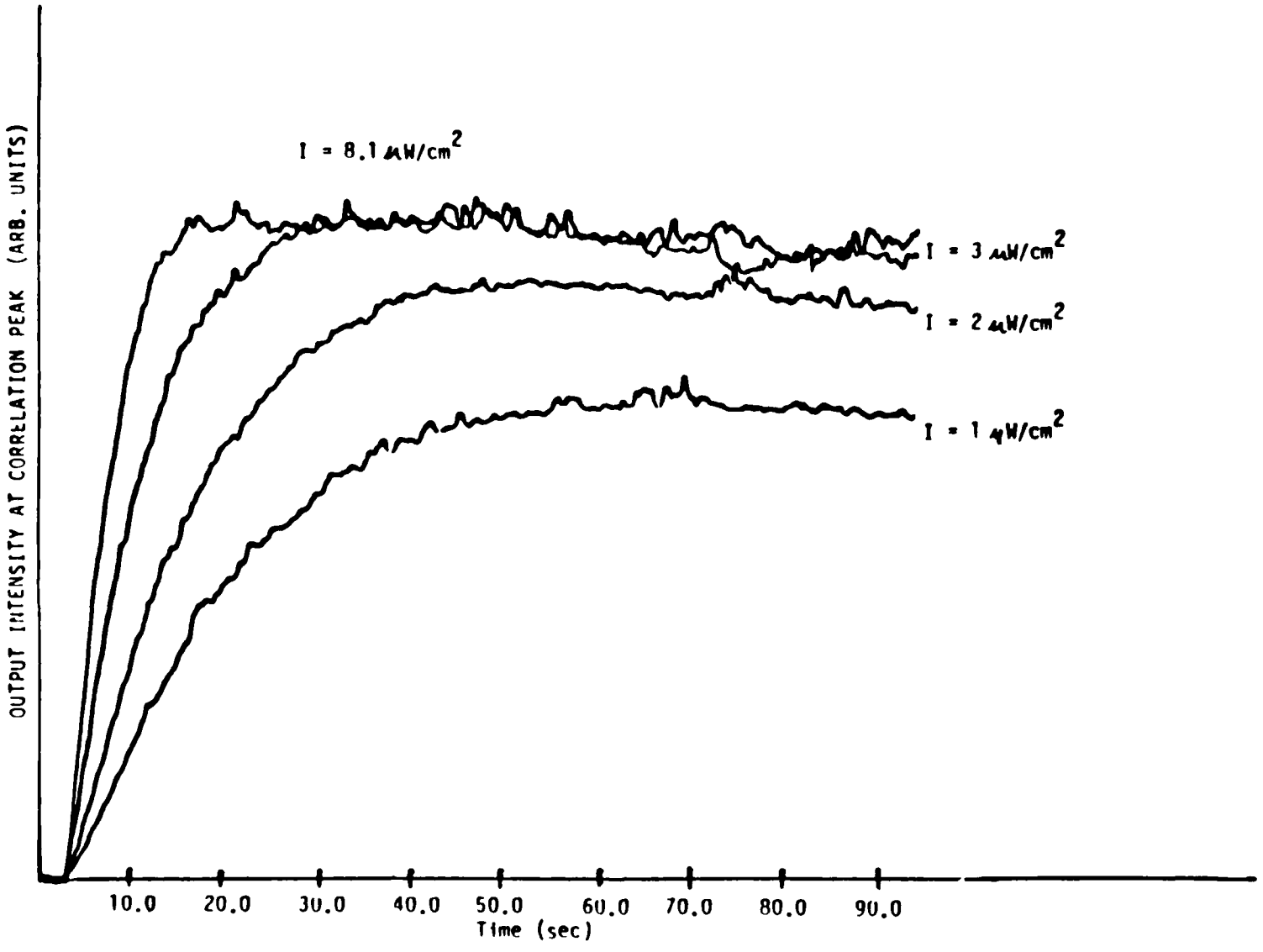

Figure 8 Output intensity at correlation peak vs time as a function of different average incident intensities.

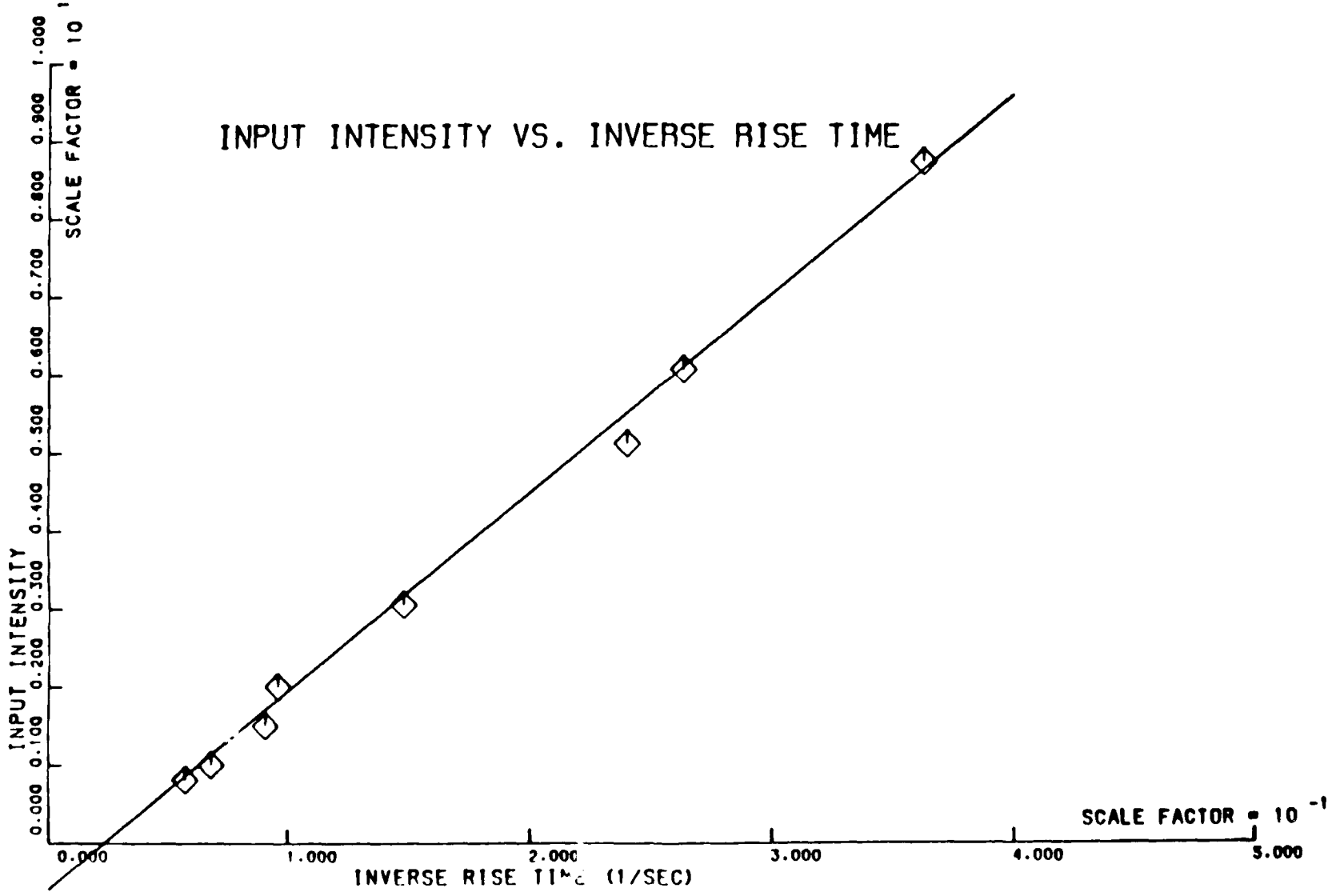

Figure 9 Inverse of the rise time vs. average incident intensity.

APPENDIX B

Adaptive Acoustooptic Processor

Demetri Psaltis and John Hong
Department of Electrical Engineering, California Institute of Technology
Pasadena, Calif. 91125

Abstract

Space-integrating, acoustooptic processors for adaptive, temporal filtering are examined. The basic architecture is then extended to the space-time domain for application in broadband phased array processing. An acoustooptic processor capable of such 2-dimensional, adaptive processing is described.

I. Introduction

A major portion of optimum filtering theory concerns itself with the efficient separation of useful signals from additive noise. Fixed optimum filters, such as the Wiener filter, are applicable when the signal and noise statistics are stationary and known apriori; the lack of such apriori knowledge, however, motivates the implementation of adaptive filters which estimate the required signal and noise characteristics. The implementation of such filtering techniques requires a processor which must be able to compute various correlation functions of signal and noise and change its transfer function accordingly.

The situation becomes considerably more complex when one is required to adaptively filter signals in the space-time domain, as in the case of broadband array processing. The number of broadband jammers that an adaptive processor can cancel without compromising its directional discrimination can be used as its performance measure. Electronic implementations of such array processors[1] have exhibited limited performance with respect to this measure. The transversal filters responsible for temporally filtering the outputs from the array elements are of low order and hence, operation is usually limited to narrowband signals, due to hardware limitations.

The bandwidth requirements and the parallel nature of array processing make optical implementations attractive. Various optical implementations have been explored by researchers in the area[2,3]. In a recent paper[4], we described two optical adaptive filters for use in the time domain. These implementations are strictly one-dimensional, requiring only one dimensional devices, permitting an extension to the space-time domain through the use of multi-channel AOD's. In this paper, we briefly review the operation of the temporally adaptive acoustooptic filter. After this foundation has been established, an adaptive array processor utilizing multi-channel AOD's in a space integrating architecture will be described.

II. Adaptive Temporal Filters

To be adaptive, a processor that optimizes either the mean-square error or SNR criterion must compute various correlation functions of the input signal and noise and vary its filter response characteristics accordingly. Specifically, we will consider situations where the signal is broadband and the additive noise consists of strong, narrowband jammers whose frequencies are unknown; the jammer frequencies must be estimated for effective noise rejection.

Shown in Fig.1 is a system diagram of the Passive Processor which was shown to adaptively perform an approximate Wiener filtering operation[4]. The operation of the system can be explained heuristically in the following manner. Suppose that the input consists solely of a single sinusoid, and consider the feedback signal, $\hat{x}(t)$, with the loop opened at the summing junction. The input sinusoid is first convolved with a replica of itself, delayed by σ to produce another sinusoid of the same frequency, also delayed by σ, at the input of the correlator. This is then correlated with the input delayed by σ to produce a sinusoid with the same phase as the input sinusoid appearing at the summing junction, the delays, σ, cancel out due to the cascaded correlation-convolution operations. The possibility of stable cancellation is now apparent since the two signals, the input and feedback signals, which are subtracted at the junction, are identical in frequency and phase. Cancellation does not occur for a broadband input, because it correlates poorly with delayed versions of itself, resulting in a negligible feedback signal, $\hat{x}(t)$. The passive processor thus discriminates against narrowband components of the input signal, while preserving the desired, broadband components of the input, making it suitable for signal estimation.

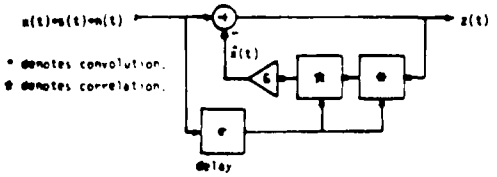

Fig.1 Passive Processor

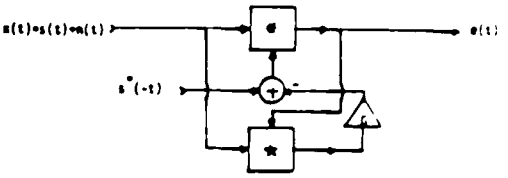

Fig.2 Active Processor

For signal detection, where a known broadband signal is to be detected amidst an additive collection of narrowband jammers of unknown frequencies, a different system is required. Shown in Fig. 2 is a system diagram of such a system, the Active Processor, along with a brief, mathematical description of its operation; a complete description can be found in reference 4. As with the Passive Processor, the basic operation of this system can be understood using heuristic arguments. Suppose that the input consists soley of a large amplitude sinusoid of frequency f_0, and the desired waveform, s(t), is a broadband signal. With the loop opened at the summing junction, the output, e(t), will consist mostly of a sinusoid of frequency f_0; this signal is then correlated with the input to produce another sinusoid of the same frequency at the summing junction. When the loop is closed, the output sinusoid resulting from the convolution of the input and the code waveform, s(t), is 180° out of phase with that which is produced by the feedback signal, and hence, cancellation of the sinusoid takes place. Again, the feedback signal is negligible for small amplitude broadband signals.

Both the Passive and Active systems require convolution and correlation as the basic building blocks. In choosing the architecture to be used, we consider the following important requirements: 1)wide bandwidth, 2)dynamically controllable convolver and correlator, 3)convolver - correlator compatibility, 4)large dynamic range. These considerations lead us to choose a space-integrating acoustooptic architecture.

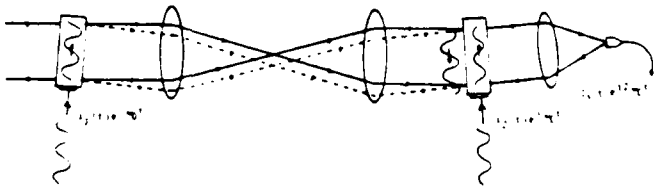

Fig.3 Space-Integrating Acoustooptic Convolver

Convolution can be performed with two AOD's as shown in Fig.3. The diffracted signal from the first AOD is imaged with unity magnification onto the second and, in the coherent realization shown, the diffracted components are spatially integrated onto a single detector whose output photocurrent is

$$I_1(t) = \int_{-T/2}^{T/2} i_1(t+\tau)i_2(t-\tau)d\tau, \quad \tau=x/v, \ T=W/2. \tag{1}$$

$i_1(t)$ and $i_2(t)$ are the complex amplitudes of the AOD input signals, v is the acoustic velocity in the AOD, and W is the physical length of the AOD aperture. This integral can be manipulated to yield the more familiar form:

$$I_1(t) = \int_{t-T/2}^{t+T/2} i_1(\tau)i_2(2t-\tau)d\tau, \tag{2}$$

which is recognized to be a finite window convolution, time-compressed by a factor of two. The seemingly troublesome compression is actually an advantage in this case as will be apparent when we consider the correlator implementation.

Correlation can be performed with the convolution configuration just described by time-reversing the input to one of the AOD's. This, however, is not acceptable for real-time operation. Shown in Fig.4 is a space-integrating processor which provides the relative motion between the two input signals that is required for correlation by using a demagnifying system between the two AOD's. The diffracted light from the first AOD is imaged with a 2:1 magnification onto the second AOD, and the diffracted light from both AOD's is spatially integrated onto a single detector. If the input to the second AOD is time-compressed by a factor of two, i.e., $i_4(t) = i_5(2t)$, then the correlator yields

$$I_2(t) \propto \int_{-T/4}^{T/4} i_3^*(t+2\tau) i_4(t+\tau) d\tau = \int_{t-T/2}^{t+T/2} i_3^*(\tau) i_5(t+\tau) d\tau, \qquad (3)$$

as its output. The above is seen to be a finite window correlation of the two signals, $i_3(t)$ and $i_5(t)$. The advantage of obtaining the time compressed output from the convolver is now clear, since it can be used as the input to the correlator just described and thus obtain a consistent, cascaded convolution-correlation operation.

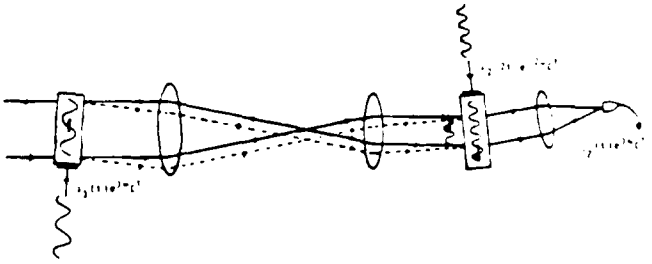

Fig.4 Space-Integrating Acoustooptic Correlator

The optical implementations of the Passive and Active Processors are shown in Figs. 5 and 6, respectively, and they differ only in their electrical interconnections. Fig. 5(6) is the system of Fig.1(2) with the optically implemented blocks of Figs. 3 and 4. In both cases, the upper branch of the processor computes the correlation while the lower performs the convolution. Since the convolver and correlator have a common input, the first AOD is shared. A more detailed description can be found in the previous publication[4].

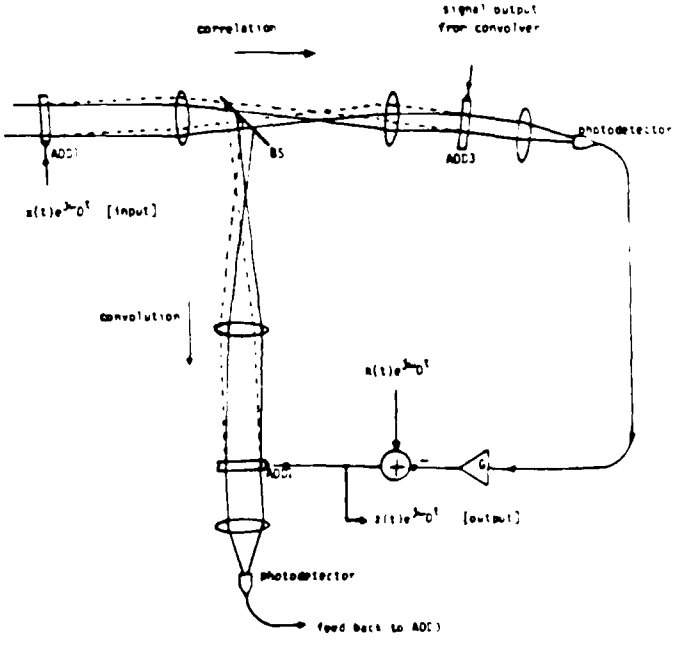

Fig.5 Adaptive Optical Processor (Passive)

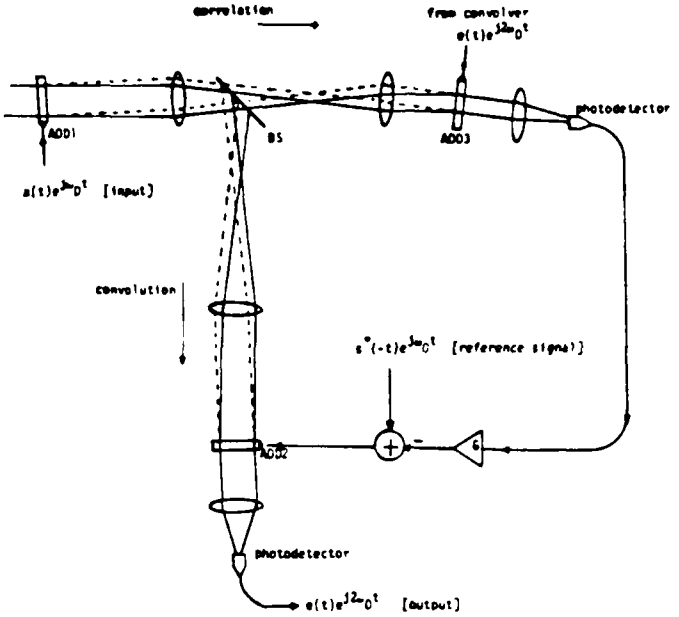

Fig.6 Adaptive Optical Processor (Active)

III. Adaptive Acoustooptic Array Processor

A general adaptive scheme is shown in Fig.7 in which each channel corresponding to one array element is filtered by a transversal filter with n controllable tap weights; if the array has N antenna elements, then the array processor requires the adaptive control of nN independent weights. Therefore, the computational load for broadband adaptive phased array processing is much heavier than that for adaptive temporal filtering because here, the array processor must adapt in two independent dimensions: space and time.

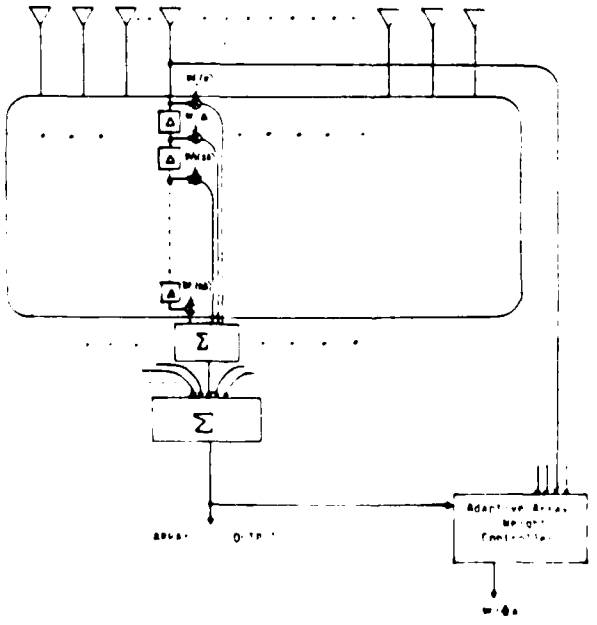

Fig.7 General Adaptive Array Processing Scheme

Optical processors are particularly attractive candidates for adaptive broadband array signal processing because of their inherent, multidimensional processing capability. Moreover, the broadband requirement can be met by the use of broadband multi-channel AOD's; the large time-bandwidth products that are available translate to the possibility of implementing very high order transversal filters. The acoustooptic processor which we now describe is an extension of the active temporal processor described earlier, to the space-time domain. Here, we employ a combination of multi and single channel AOD's to perform the required operations.

The output of a general, space-time filter, with a finite accumulation time can be expressed as

$$y(t) = \sum_{i=1}^{N} \int_{-T/2}^{T/2} x_i(\tau) h_i(t-\tau)\, d\tau, \tag{4}$$

where $x_i(t)$ is the signal from the ith antenna element, and $h_i(t)$ is the filtering function in each channel. A similar expression is obtained for the optically implemented space-time filter using two multi-channel AOD's shown in Fig.8. The output of this filter is

$$y(t) = \sum_{i=1}^{N} (1/T) \int_{-T/2}^{T/2} x_i(t-\tau) h_i(t+\tau)\, d\tau, \tag{5}$$

and we see that the only difference from the general filter (Eq.4) is in the time compression of the output. It can be shown that the optimum choice for $h_i(t)$ in Eq.(5) satisfies the system of integral equations:

$$\sum_{j=1}^{N} \int_{-T/2}^{T/2} h_j^*(t+\tau') \gamma_{ij}(\tau-\tau')\, d\tau' = \lambda s_i(t-\tau), \tag{6}$$

where $s_i(t)$ is the desired signal vector and $\gamma_{ij}(t)$ is the covariance matrix of the input noise given by

$$\gamma_{ij}(\tau) = E\,[n_i(t) n_j^*(t-\tau)]. \tag{7}$$

$n_i(t)$ is the noise vector appearing at the array elements.

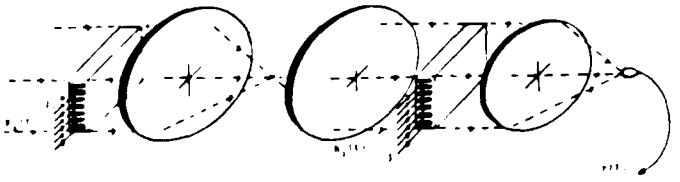

Fig.8 Acoustooptic Space-Time Filter

For adaptivity, we need to calculate and continuously update the filter function $h_i(t)$ to drive the output to the optimum result. As with the previously described Active Processor, the output must be correlated with the input to produce the appropriate filter function. Since the array processor has n inputs and one output, this requires that we correlate n signals with a common one. This can be achieved with the arrangement shown in Fig.9 which shows the use of a multi-channel AOD driven by the n antenna element outputs, in conjunction with a single channel AOD which is driven by the array output signal. Specifically, the output of the ith element of the linear detector array of the correlator is given by

$$r_i(t) = (1/T) \int_{-T/2}^{T/2} y(t+\tau) x_i^*(t+2\tau) d\tau. \tag{8}$$

For proper correlation to appear at each output, the signal driving the single channel AOD must be time-compressed by a factor of two. This is indeed the case for the system described, and thus, the AOD implemented space-time filter and the n-channel correlator with a single reference are compatible.

Shown in Fig.10 is the array processor system diagram that shows the interconnections that are required; it is a direct extension of the Active Processor to 2-dimensions. The output from each antenna element is correlated with the processor output to produce the filter function for that element. The steering vector, $s_i(-t)$, determines the look

direction of the array and also is the temporal reference signal used for the detection of the desired signal, s(t). It can be derived by feeding a tapped delay line with s(t); the output from the ith tap corresponds to $s_i(t)$ and the tap spacing is adjusted to obtain the proper look direction:

$$s_i(t) = s(t-i\Delta) = s(t-i(d/c)\cos\theta), \tag{9}$$

where θ is the desired look angle from boresight, d is the array element spacing, and c is the speed of light.

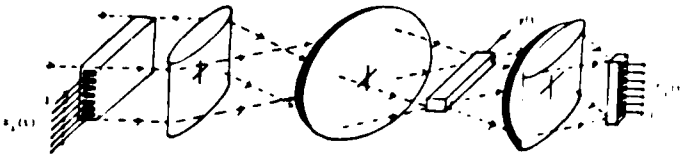

Fig.9 Multi-Channel Acoustooptic Correlator

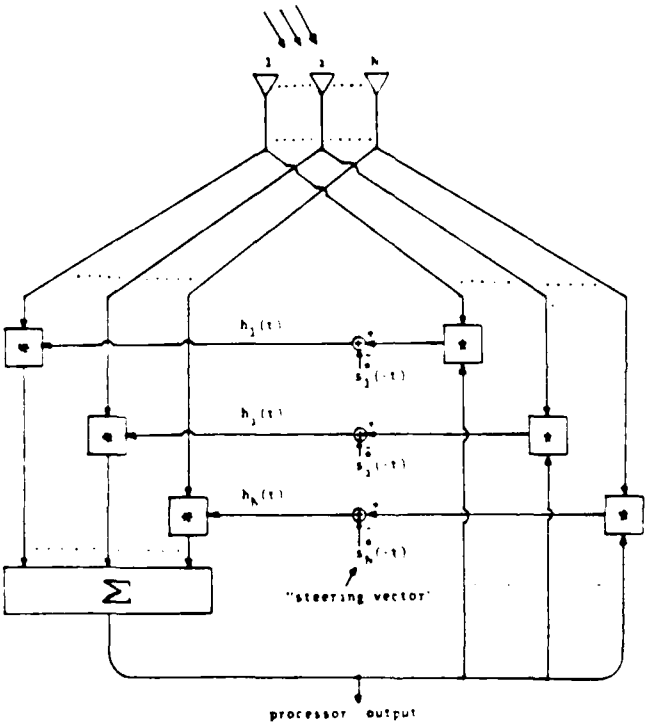

Fig.10 Broadband Adaptive Array Processor

Fig.11 shows the optically implemented adaptive array processor with the AOD-implemented space-time filter in the upper branch and the n-channel correlator in the lower one. By combining Eqs.(7) and (8), the equation that determines the filter function, $h_i(t)$ is seen to be

$$h_i(t)=s_i^*(-t)-(G/T^2)\sum_{j=1}^{N}\int\!\!\int_{-T/2}^{T/2} x_i^*(t+2\beta)x_j(t-\tau+\beta)h_j(t+\tau+\beta)\,d\beta\,d\tau, \tag{10}$$

where G is the feedback gain. Under conditions of low input SNR and large feedback gain[4], Eq.(10) can be transformed to the frequency domain to yield

$$(G/4\pi^2)\sum_{j=1}^{N} B_j(\omega)\int_{-\infty}^{\infty} N_i^*(\omega_1)N_j(\omega_1)\,\mathrm{sinc}^2[(\omega-\omega_1)T/(2\pi)]\,d\omega_1 \cong S_i^*(\omega), \tag{11}$$

For comparison, consider the Fourier Transform of Eq.6; when the accumulation time is infinite, the optimum filter equation is given by

$$2\sum_{j=1}^{N} \Gamma_{ij}(\omega)H_j(\omega) = \lambda^{\circ}S_i^{\circ}(\omega), \qquad (12)$$

$$\Gamma_{ij}(\omega) = \text{F.T.}\ [\ \gamma_{ij}(\tau)\ ],$$

where $\Gamma_{ij}(\omega)$ is the spectral density matrix. Identifying the integral in Eq.11 as the smoothed estimate of the spectral density matrix of the input noise vector, Eq. 11 is approximately equivalent to Eq.12. The effect of the finite time integration window is seen in the smoothing of the noise spectrum.

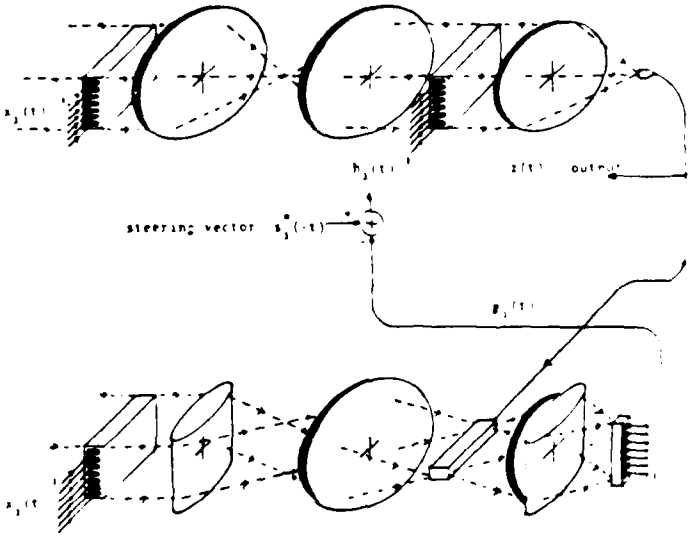

Fig.11 Adaptive Acoustooptic Phased Array Processor

Acknowledgement

This work is supported by the Rome Air Development Center and, in part, by the Air Force Office of Scientific Research.

IV. References

1. R. Riegler and P. Compton, Jr., 'An Adaptive Array for Interference Rejection, Proc.IEEE 61,748 (1973).

2. J. F. Rhodes,'Adaptive Filter with a Time-Domain Implementation Using Correlation Cancellation Loops,' Appl.Opt.22, 282 (1983).

3. A. Vanderlugt, 'Adaptive Optical Processor,' Appl.Opt.21, 4005 (1982).

4. D. Psaltis and J. Hong, 'Adaptive Acoustooptic Filter,' Appl.Opt.23, 3475 (1984).

APPENDIX C

Acoustooptic Adaptive Signal Processing

John Hong and Demetri Psaltis
California Institute of Technology, Department of Electrical Engineering
Pasadena, California 91125

Abstract

Acoustooptic methods for adaptive filtering of temporal signals are discussed. Two specific architectures are presented: one utilizing space-integration alone and the other combining both time and space integrating techniques. Performance issues regarding the space-integrating system are discussed in detail, and a description and experimental results for the space-time integrating filter are presented.

Background

Optimal filtering in unknown or time-varying signal environments requires the use of systems which can compute the necessary noise characteristics and adapt to yield approximately optimum performance. In this paper, the case of broadband signals received in the presence of strong, additive, narrowband jammers whose spectra are unknown is considered. This situation is illustrated in Fig.1, showing the useful broadband signal overwhelmed by a strong jammer. If the spectral density of the jammer were known apriori, then the Wiener filter whose transfer function is given by[1]

$$H(\omega) = \frac{S_s(\omega)}{S_s(\omega) + S_n(\omega)}, \tag{1}$$

would be used to yield the optimum performance in the least mean square error sense ($S_s(\omega)$ and $S_n(\omega)$ are the spectral densities of the signal and uncorrelated jammer noise, respectively). In the case of interest, the noise spectrum is unknown and must therefore be computed and the system response adjusted accordingly to approximate the Wiener filter.

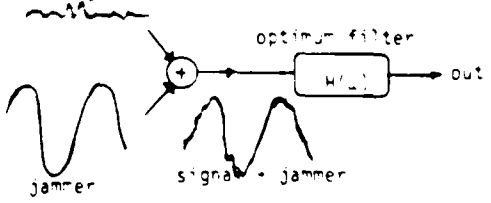

Fig.1 Optimum Filtering

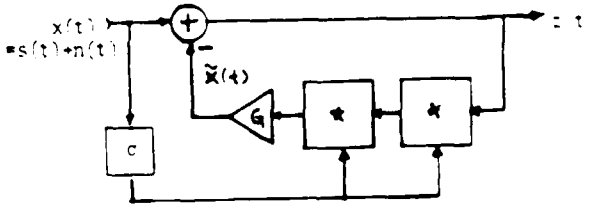

Fig.2 Passive Processor

Several optically implemented adaptive systems have previously been proposed.[2,5,6,8] A block diagram of the adaptive system discussed in this paper is shown in Fig.2. The system has been described in detail in a previous publication[4], and its operation is briefly reviewed here. The two major components of the system are the convolution and correlation blocks (indicated by • and ★, respectively, in Fig.2). The outputs of the convolver and correlator blocks are related to their inputs by

$$u(t) = \int_{-\infty}^{\infty} s_1(t-\tau)\, s_2(\tau)\, d\tau,$$
$$w(t) = \int_{-\infty}^{\infty} s_3(t+\tau)\, s_4^*(\tau)\, d\tau, \tag{2}$$

respectively, where $s_i(t)$ denote the inputs to the blocks. The processor discriminates between narrowband signals which correlate well with delayed versions of themselves and broadband signals which correlate poorly. Thus, with the loop open at the summing node, the feedback signal $\tilde{x}(t)$ for an input consisting entirely of a broadband signal is negligibly small because such an input correlates poorly with delayed portions of itself. This is contrasted to the case where the input is a sinusoid, in which case the convolution of the input with itself delayed, followed by a correlation with the input delayed by the same amount yields a sinusoid of the same frequency and phase as the input. When the loop is closed, broadband components of the input feed through unaffected while suppression of correlated portions takes effect. The following approximate input-output relationship can be derived for the filter in Fig.2[4].

$$z(t) \approx x(t) - G\iint_{-\infty}^{\infty} z(\tau) n^*(\alpha-\sigma) n(t+\alpha-\tau-\sigma)\, d\alpha d\tau, \tag{3}$$

where z(t) is the output, n(t) is the input jammer noise, and x(t) = s(t) + n(t) is the total input. A simple interpretation is found by the Fourier transformation of the above equation, resulting in the following 'transfer' function:

$$\frac{Z(\omega)}{X(\omega)} = \frac{1}{1 + G\,|N(\omega)|^2} \,. \tag{4}$$

where Z(ω), X(ω), and N(ω) are the Fourier transforms of z(t), x(t), and n(t), respectively. If the jammer spectrum is sharply peaked at certain frequencies, the processor serves to suppress these components by an inverse filtering operation.

Space Integrating (SI) Optical Processor

A. Description

An acoustooptic convolver can be implemented using the SI architecture shown in Fig.3. The specific set up shown in Fig.3 is a coherent version of a geometry which can just as easily be implemented using incoherent techniques. The light diffracted from AOD1 is imaged onto AOD2, resulting in two counter-propagating signals at the exit plane of AOD2. These field amplitudes are then spatially integrated by lens L3, and the integrated signal is detected by the photodetector to yield the photocurrent, with a component proportional to:

$$I_1(t) = (2/T) \int_{-T/4}^{T/4} i_1(t+\tau)\, i_2(t-\tau)\, d\tau, \quad T=W/v, \ \tau=x/v, \tag{5}$$

where v is the acoustic velocity in the AODs, and W is the aperture of the AOD. A change of the integration variable leads to a more familiar form given by

$$I_1(t) = (2/T) \int_{t-T/2}^{t+T/2} i_1(\tau)\, i_2(2t-\tau)\, d\tau. \tag{6}$$

which is recognized to be a finite window convolution, time-compressed by a factor of two. The complication of this time compressed output becomes an advantage when considering the implementation of the correlator.

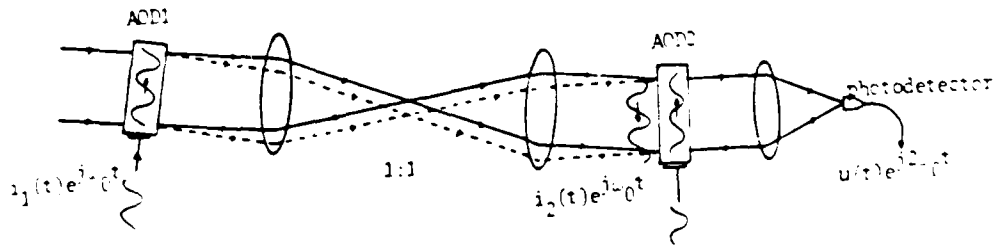

Fig.3 Space Integrating Convolver

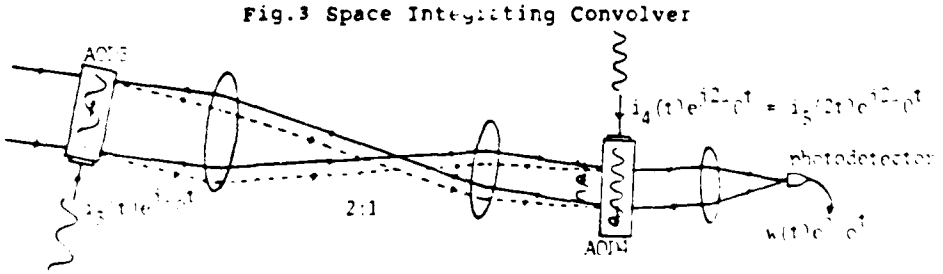

Fig.4 Space Integrating Correlator

Correlation can be performed by the set up shown in Fig.3 if one of the input signals is time-reversed. Since this is incompatible with real-time operation, a different geometry, one that is compatible with the time-compressed output of the convolver, is examined. Correlation requires that the input signals slide past each other without coordinate inversion. This is achieved by the implementation shown in Fig.4 in which the diffracted light from the first AOD is imaged with a 2:1 demagnification onto the second AOD. At the exit plane of the second AOD, the two acoustic signals are co-propagating with different velocities because of the demagnification. These signals are then spatially

integrated onto a single detector. If the input signal to the second AOD is time compressed by a factor of two, i.e., $i_4(t) = i_5(2t)$, then the correlator output is

$$I_2(t) = (2/T)\int_{-T/4}^{T/4} i_3^*(t+2\tau)i_4(t+\tau)d\tau = (2/T)\int_{t-T/2}^{t+T/2} i_3^*(\tau)i_5(t+\tau)d\tau. \quad (7)$$

The above is the desired finite window correlation of the two signals, $i_3(t)$ and $i_5(t)$. Since the output of the convolver in Fig.3 is indeed time-compressed by a factor of two, it can be used to drive the second AOD of the correlator, resulting in the cascaded correlation-convolution operation that is required in the passive processor.

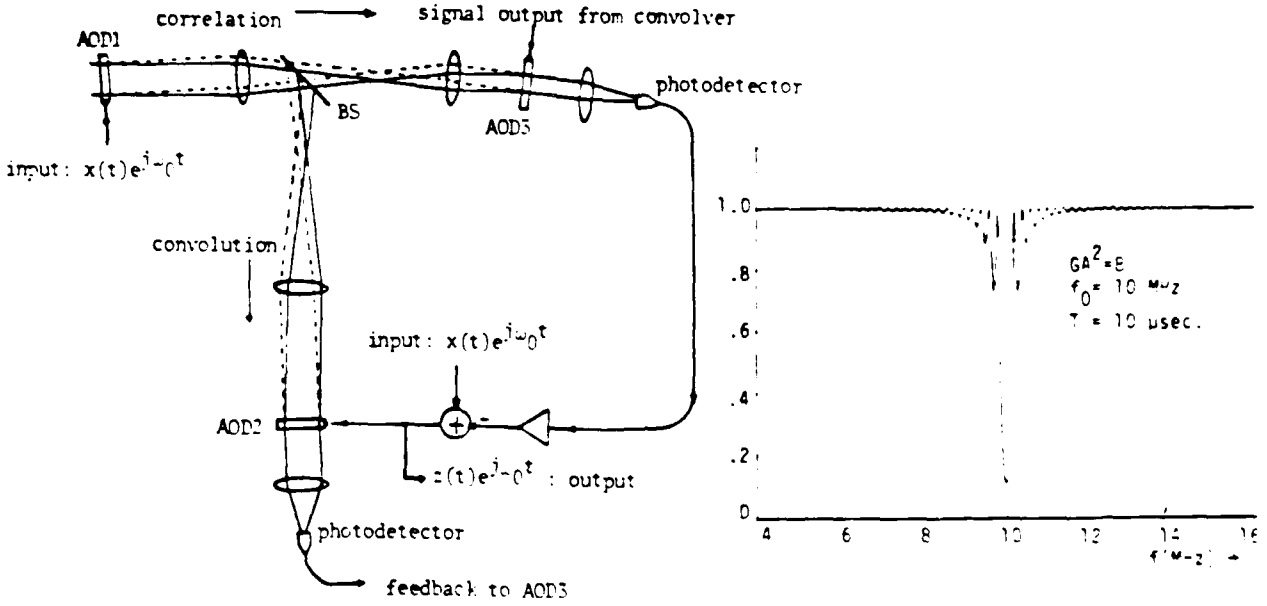

Fig.5 Space Integrating Adaptive Optical Processor

Fig.6 Freq.Response to One Jammer

Shown in Fig.5 is the complete processor. Since the correlator and convolver have one common input, one AOD can be shared by the two blocks, resulting in a system requiring only 3 devices. The input-output equation describing the processor in Fig.5 is given by

$$z(t) = x(t) - (4G/T^2)\int\int_{-T/4}^{T/4} x^*(t+2v)x(t+\tau+v)z(t-\tau+v)d\tau dv, \quad (8)$$

where x(t) is the input to the system and z(t) the output. For $x(t) = s(t) + n(t)$, where n(t) is the narrowband jammer and s(t) the broadband signal, the above equation can be Fourier transformed to yield

$$\frac{Z(\omega)}{X(\omega)} = \frac{1}{1 + (G/\pi^2)\int_{-\infty}^{\infty} |N(\alpha)|^2 \mathrm{sinc}^2[(\omega-\alpha)T/4\pi]d\alpha}. \quad (9)$$

The above 'transfer' function has the form of the inverse filter described earlier, except that the noise spectrum is smoothed by a sinc function due to the finite time windows of the AODs.

B. Performance

The optical system described thus far was implemented for preliminary study. Jammer suppression was successfully observed; however, the maximum, stable null depth obtained was limited to 7dB. It is important to theoretically characterize the performance limits of the processor in terms of system parameters such as the AOD aperture size and detector noise before we attempt to systematically improve the performance level. Three important

issues are discussed: 1) the resolution with which the processor discriminates against jammers, 2) null depth limitations due to detector noise, and 3) transients in the system response due to the delays inherent in the system.

The resolution of the system is characterized entirely by the size of the AOD apertures for they determine the length of the signal sample at any one time. When the input consists of a single sinusoid at frequency ω_0 and amplitude A, the exact form for the Fourier transform of the output can be determined from Eq.8 to be

$$Z(\omega) = \frac{X(\omega)}{1 + GA^2\ \mathrm{sinc}^2[(\omega-\omega_0)T/4\pi]}\ , \qquad (10)$$

where $Z(\omega)$ and $X(\omega)$ are the Fourier transforms of the output and input signals, respectively. A plot of $Z(\omega)$ for $GA^2 = 8$, $T = 10$ μsecs., and $\omega_0/2\pi = 10$ MHz is shown in Fig. 6. The sidelobe structure is entirely due to the finite apertures of the AODs. The sidelobes can be reduced at the cost of widening the null at the jammer frequency by introducing apodization functions through the appropriate illumination of the AODs. The issue of apodization will be examined more closely later in the discussion of transients and stability.

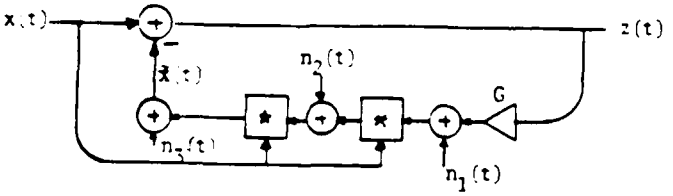

Fig.7 System Noise Model

While the finite apertures determine the resolution of the processor, the maximum nulling depth is governed by other mechanisms. In order to better understand this limitation, the deterioration in the cancellation of one jammer, $n(t) = Ae\exp(j\omega_0 t)$, due to the system noise contributed by the detectors and amplifiers is now studied. The system model depicting the noise sources is shown in Fig.7, where $n_1(t)$ is the noise from the feedback amplifier while $n_2(t)$ and $n_3(t)$ correspond to those arising from the photodetectors in the convolver and correlator, respectively. The noise processes are assumed to be independent, stationary, complex gaussian processes[3], each with variance σ^2. Since the input is a single frequency jammer, the convolver and correlator behave as narrow-bandpass filters centered at that frequency. If the space bandwidth products of the convolver and correlator are larger than the feedback gain, the contribution of the noise sources $n_1(t), n_2(t)$, filtered by the convolver and correlator is negligible compared to $n_3(t)$ which is added directly onto the feedback signal $\tilde{x}(t)$. The portions of noise which are fed back are suppressed by the correlator and convolver and can be neglected to first order. Thus, only the noise due to $n_3(t)$ appears directly at the output. We expect that the performance limit set by the system noise would not be reached unless the jammer amplitude is suppressed to σ, the noise level. In our experiments, however, the jammer in the output signal was clearly stronger than the system noise, showing that the noise performance limit was not reached.

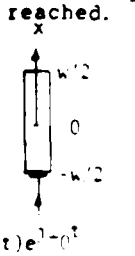

Fig.8 AO Delays

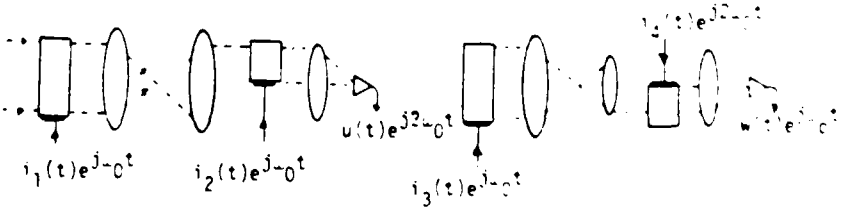

Fig.9 Delay Modified Convolver and Correlator

A more severe limitation can arise from the time delays that exist in the AODs. Shown in Fig.8 is an AOD with the spatial coordinate, x, centered on the AOD. If an electrical signal s(t) is used to drive the AOD, then the amplitude of the acoustic wave in the AOD is proportional to $s(t-x/v-T/2)$, where T is the total aperture time. This effectively introduces time delays to appear in the feedback path which can cause instabilities in the processor. To minimize the delays, the AODs in the convolver and correlator can be shifted in space as described in Fig.9 to result in the following convolver and correlator input output equations, including the delays:

$$\text{convolver:}\quad u(t) = (4/T)\int_0^{T/4} i_1(t-T/2+\tau)\,i_2(t-\tau)\,d\tau, \qquad (11)$$

correlator: $w(t) = (4/T) \int_{-T/4}^{0} i_3^*(t-T/2+2\beta) i_4(t+\beta)\, d\beta$.

The resulting modified system is described by the following equation:

$$z(t) = x(t) - 16(G/T^2) \int_{-T/4}^{0} \int_{0}^{T/4} x^*(t-T/2+2\beta)x(t-T/2+\tau+\beta)z(t-\tau+\beta)d\tau d\beta. \quad (12)$$

For a single jammer input, $x(t) = Ae\exp(j\omega_0 t)$, the above can be transformed to give the following, exact frequency domain result:

$$Z(\omega) = \frac{X(\omega_0)}{1 + GA^2\, \mathrm{sinc}^2[(\omega-\omega_0)T/8\pi]\exp[-j(\omega-\omega_0)T/4]} . \quad (13)$$

The phase factor present in the denominator is due to the delays. The consequence of this phase factor is that the denominator is no longer positive for arbitrarily large values of G. In fact, the denominator vanishes for $(\omega-\omega_0)T/4 = \pi$ with $G = G_c = \pi^2/4A^2$, indicating instability for gain values larger than G_c which corresponds to an amplitude suppression of only 10dB. This value of maximum suppression is verified by computer simulations of the processor response to a step input. Fig.10 shows the envelope of the response of the processor to a unit step jammer input, for G=1, and G=2.5, which is near the critical value, G_c. The initial constant portion of the response is due to the delays in the convolver and correlator. Indeed, the second plot shows an oscillatory behavior, indicating marginal stability.

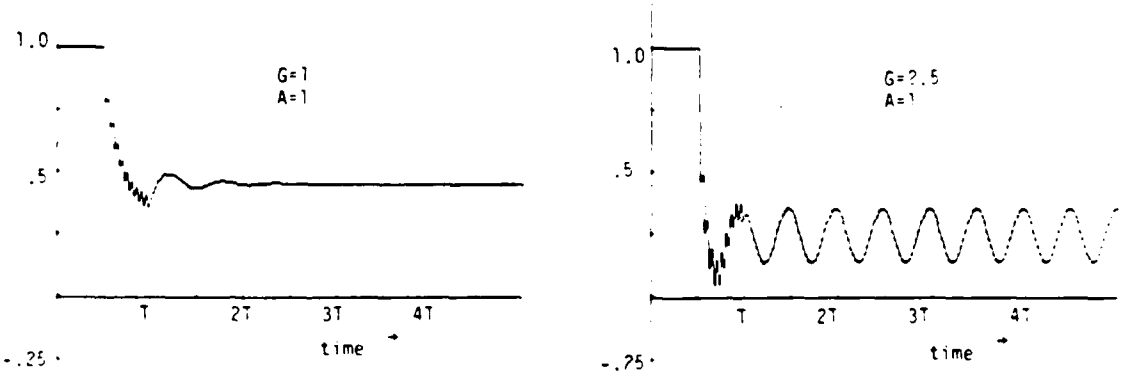

Fig.10 Step Response

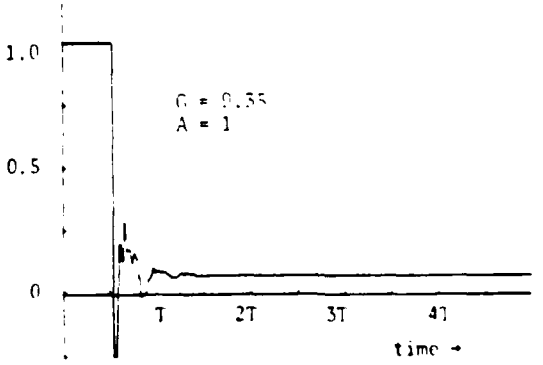

Fig.11 Step Response with Exponential Apodization

The low critical gain stems from the rather large sidelobes of the sinc^2 function coupled with the phase factor due to the delays. At the cost of loss in resolution, the sidelobes can be reduced by apodizing the AOD windows, resulting in systems which can tolerate higher feedback gains while remaining stable. As a simple example, the effect of an exponential tapering function was evaluated by computer simulations. Shown in Fig.11 is the step response obtained with exponential apodization. Convergence is still rapid, and

the suppression is improved to 20dB. Other tapering functions may yield stable nulling performance to match that predicted by the system noise considerations as discussed earlier but at the cost of loss in resolution.

Space-Time Integrating Optical Processor

In the SI system, the desired correlation function is formed by a SI correlator and read out with a SI convolver. Alternative approaches where integration in both time and space are used have been described by Rhodes[5] and Penn[6]. In such systems, the correlation integral is computed by a time-integrating spatial light modulator (SLM) and read out with a space-integrating convolver. We now consider an implementation using the photorefractive crystal BSO as the time-integrating SLM. The advantages of this implementation over the previous ones[5,6] which used the Hughes liquid crystal light valve and a phosphor screen, respectively as the time-integrating SLMs are: 1)the system response speed is easily controllable since the response time of the photorefractive effect depends on the exposure level. 2)a coherent implementation is possible. 3)higher resolution is exhibited by the photorefractive devices. 3)since the crystal does not respond to DC or bias levels, the implementation will not suffer from bias build-up problems common among time-integrating systems. 4)the photorefractive devices are simpler since they require only the crystal and a voltage source to supply the external field which is required for some crystals.

The photorefractive effect can be understood in the following way. Two writing beams of light which are spatially modulated with information intersect in the crystal to form an intensity grating pattern. Because of the spatially varying intensity pattern, the charge carriers in the crystal redistribute themselves into a space-charge grating. The electric field associated with this charge grating accordingly modulates the refractive index of the crystal through the electrooptic effect, allowing the read-out of the written information by a third beam. A property characteristic of this effect is that the response time is inversely proportional to the average writing beam intensity impinging on the crystal. This property translates to the controllability of the system response time in the present application, an added flexibility. In our experiments, the time constant was on the order of a few seconds because of the relatively low writing intensities used.

Shown in Fig.12 is a time integrating correlator that exploits the time response characteristics just described. AOD1 and AOD2 serve to spatially modulate the writing Argon laser beams with two counter-propagating signals $s_1(t-x/v)$ and $s_2(t+x/v)$; an imaging lens pair is used to image the AODs onto the BSO crystal. The index grating formed within the crystal is modulated by the correlation of the two signals. The diffracted read-out wave contains only the modulation of the index grating and is thus bias-free. It can be shown that the amplitude of the diffracted light is:

$$E_{diff}(x) \sim \int_0^t e^{(t_1-t)/\tau} s_1(t_1-2x/v-T/2)s_2^*(t_1+2x/v-T/2)\, dt_1, \qquad (14)$$

$$\sim \int_{t-2x/v-T/2-\tau}^{t-2x/v-T/2} s_1(t_2)s_2^*(t_2+4x/v)\, dt_2,$$

τ = time constant of BSO.

which is the cross-correlation function of $s_1(t)$ and $s_2(t)$ with the spatial coordinate, x, being the shift variable. This correlation can be detected by imaging the crystal onto a CCD detector array for serial read-out.

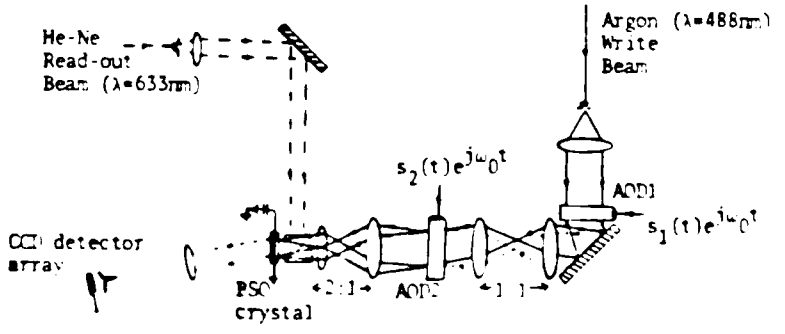

Fig.12 BSO Correlator

The incorportation of the correlator just described into the adaptive system of Fig.2 is rather simple and requires the addition of only 1 AOD with a 4:1 telescope to compensate for the 2:1 demagnification used in writing the correlation onto the BSO. The system is shown schematically in Fig.13. The output and input (z(t) and x(t), respectively) constitute the inputs to the correlator. AOD3 is also driven by the input signal and diffracts a portion of the He-Ne read beam to pass through the BSO unmodulated. The DC from AOD3, however, is Bragg matched to the index grating in the crystal and reads out the correlation function. If all of the AODs are driven at the same frequency, then the bear diffracted by the BSO crystal and that diffracted by AOD3 are collinear and interfere temporally at ω_0, the Doppler frequency introduced by AOD3. The two diffracted waves are Fourier transformed by lens L5, and the resulting intensity is detected by the photodetector. The output current is the convolution of the input, x(t), and the correlation formed inside the crystal, and it becomes the feedback signal, $\tilde{x}(t)$, which is then subtracted from the input to produce the output signal. The resulting input-output eqn. is

$$z(t) \cong x(t) - G \int_{-T/8}^{T/8} \int_{t-\tau}^{t} x^*(t'-2\alpha-T/2)x(t-4\alpha-T/2)z(t'+2\alpha-T/2)dt'd\alpha, \qquad (15)$$

which is similar to the SI system except for the presence of both space and time integrals.

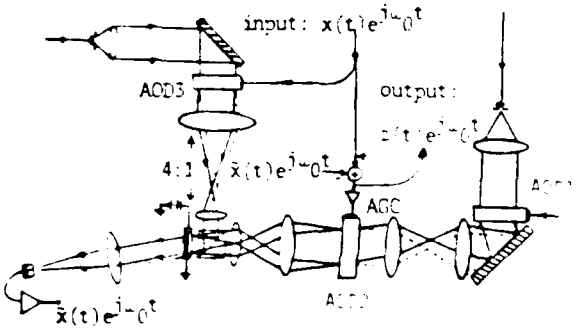

Fig.13 Space-Time Integrating Processor

One underlying assumption behind Eq.14 and hence 15 also, is that the crystal is thin enough to put the read out process into the Raman-Nath regime. This is not the case, however, and the coupling between the writing beams must be taken into account. Coupled wave theory predicts that the phase of the index grating will be a function of the ratio of the two write beam intensities, this was found to be the case experimentally. This introduces a complication in the present system because, as soon as the processor begins to suppress an incoming jammer, the output, z(t), begins to decrease in amplitude, causing the ratio of the intensities of the two write beams which emerge from AOD1 and AOD2 to diminish. This translates to a phase change in the feedback signal, possibly causing instability to appear. This can be remedied, however, by placing an AGC (automatic gain control) amplifier at the input to AOD2. As adaptation proceeds and z(t) begins to decrease, the AGC tracks the drop in amplitude to keep the input of AOD2 at a fixed value. The system just described has been set up in the laboratory for preliminary study. Shown in Fig.14 is a result showing the spectrum of the input signal, a jammer at 70 MHz, and that of the processor output. The observed suppression was about 15 dB. Better suppression can be expected as better AGC amplifiers are used.

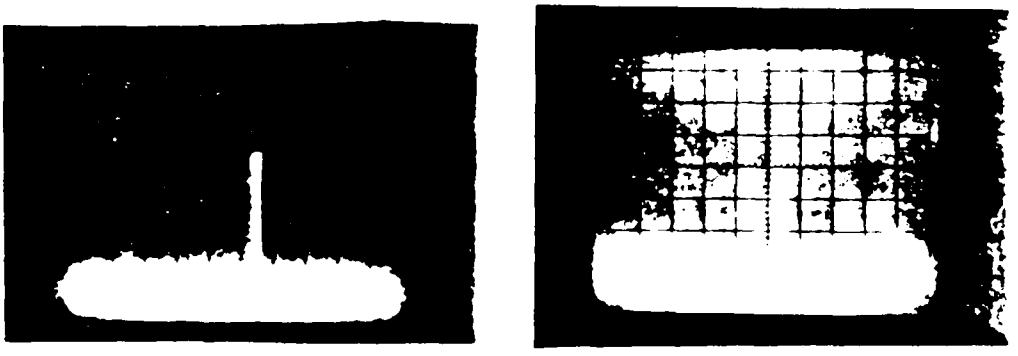

Fig.14 Suppression of Jammer (70 MHz) with BSO Processor
a) input spectrum b) output spectrum

Conclusion

Two optical implementations of adaptive signal processors were described. The space-integrating processor was shown to exhibit very fast response times but also stability problems which could be corrected to a large extent by apodization techniques. The use of such a processor would be appropriate in situations where the jammer noise is varying rapidly in time, such as in the case of blinking jammers or frequency hopped jammers. The space-time integrating system was implemented with a photorefractive BSO SLM to form the necessary correlation function in conjunction with a SI convolver for adaptive filtration. Although considerably slower that its SI counterpart, it has the flexibility of a controllable response time. Future research in photorefractive materials may yield faster crystals.

Acknowledgement

This research is supported by the Air Force Office of Scientific Research and in part by the Rome Air Development Center.

References

1. W. Davenport and W. Root, Introduction to Theory of Random Signals and Noise (McGraw-Hill, New York, 1967).

2. D. Psaltis and J. Hong, 'Adaptive Acoustooptic Filter,' Appl. Opt.23, 3475 (1984).

3. R.Arens, 'Complex Processes for Envelopes of Normal Noise,' IRE Trans.on Info.Th., IT-3, Sept.1957.

4. N.V. Kukhtarev, et al, 'Holographic Storage in Electrooptic Crystals, Parts I and II, Ferroelectrics 22, pgs.949- , (1979).

5. J.Rhodes, 'Adaptive Filter with a Time-Domain Implementation Using Correlation Cancellation Loops,' Applied Optics 22,282(1983).

6. W.A.Penn, et al, 'Acousto-optic Adaptive Processing,' Final Draft, RADC-TR-83-156, Phase Report, Dec.1983.

7. D.Psaltis, J.Yu, and J.Hong, 'Bias-free Time Integrating Correlator Using a Photorefractive Crystal,' submitted to Applied Optics.

8. A.V.Vanderlugt, 'Adaptive Optical Processor,' Appl.Opt.21,4005,(1982).

END

DTIC

7-86